Electronic Supplementary Material (ESI) for Organic & Biomolecular Chemistry.

Noncooperative Guest Binding by Metal-free [2+2] Schiff-base Macrocycles

Mohammad T. Chaudhry,[a] Brian O. Patrick,[a] Shigehisa Akine[b] and Mark J. MacLachlan[a,c,d,*]

a. Department of Chemistry, University of British Columbia, 2036 Main Mall, Vancouver, British Columbia, V6T 1Z1, Canada. E-mail: mmaclach@chem.ubc.ca

b. Graduate School of Natural Science and Technology, Kanazawa University, Kanazawa 920-1192, Japan.

c. WPI Nano Life Science Institute, Kanazawa University, Kanazawa, 920-1192, Japan.

d. Stewart Blusson Quantum Matter Institute, University of British Columbia, 2355 East Mall, Vancouver, BC, Canada, V6T 1Z4.

Table of Contents

General

All solvents and reagents were used as received unless otherwise stated. Compound **1** was prepared according to a literature procedure.[1] Single crystals of **1** were grown *via* slow evaporation of a solution of **1** in DCM at -12 ºC. All reactions were conducted under air unless stated otherwise. Dry tetrahydrofuran (THF) was obtained from an Inert PureSolv MD5 Solvent Purification System. Dry *N*,*N*-dimethylformamide (DMF) was dried over 4 Å molecular sieves and sparged with Ar to degas. Matrix compound *trans*-2-[3-(4-*tert*-butylphenyl)-2-methyl-2-propenylidene]malononitrile (dctb) was obtained from Sigma-Aldrich. Dichloromethane-d_2 (DCM-d_2) and dimethylsulfoxide-d_6 (DMSO-d_6) were obtained from Sigma-Aldrich. Chloroform-d_1 (C*D*Cl$_3$) and 1,1,2,2-tetrachloroethane-d_2 (1,1,2,2-TCE-d_2) were obtained from Cambridge Isotopes Laboratories. Flash column chromatography was carried out using SiliCycle (230-400 mesh) silica gel. Thin-layer chromatography (TLC) was carried out using Sigma-Aldrich aluminum-backed Silica TLC plates and visualized using UV light (λ = 254 nm).

Nuclear magnetic resonance (NMR) spectra were recorded on a Bruker AV-300 or AV-400 MHz spectrometer, and chemical shifts (δ) were referenced to the residual proton signal of the employed deuterated solvent. Mass spectra (MS) were obtained using electrospray ionization (ESI) on a Bruker Esquire-LC ion trap mass spectrometer equipped with an electrospray ion source or a matrix-assisted laser desorption/ionization (MALDI) equipped with a Bruker Biflex IV time-of-flight (TOF) mass spectrometer. High-resolution mass spectra were obtained using an ESI-TOF Waters Micromass LCT spectrometer. Ultraviolet-visible (UV-vis) spectra were obtained on a Varian Cary 5000 UV-vis-near-IR spectrophotometer using a 1 cm pathlength quartz cuvette. Emission spectra were obtained on a Photon Technology International (PTI) QuantaMaster 50 spectrophotometer utilizing a 75 W Xenon arc lamp.

Single crystal X-ray diffraction (SCXRD) data were obtained using a Bruker APEX X8 or DUO instrument, equipped with a graphite monochromated Mo Kα radiation (λ = 0.71073 Å) or Cu Kα radiation (λ = 1.5406 Å). Data were processed using Bruker APEX3,[2] and an error model was completed using SAINT V8.38.[3] Structure solutions were done using SHEL-XT with the intrinsic phasing method.[4] Structure refinement was done using SHEL-XL using the least-squares method.[5] Both solution and refinement were done using the OLEX2 interface.[6] All non-hydrogen atoms were modeled anisotropically, with hydrogen atoms being modeled isotropically. Hydrogen atoms were also modeled with geometric constraints for bond lengths and angles. Graphical representations of CIF data were prepared using CrystalMaker®.[7] Compound **4** crystallized as a modulated structure and was solved and refined using Jana2006.[8]

Spectral data for compounds

NMR data

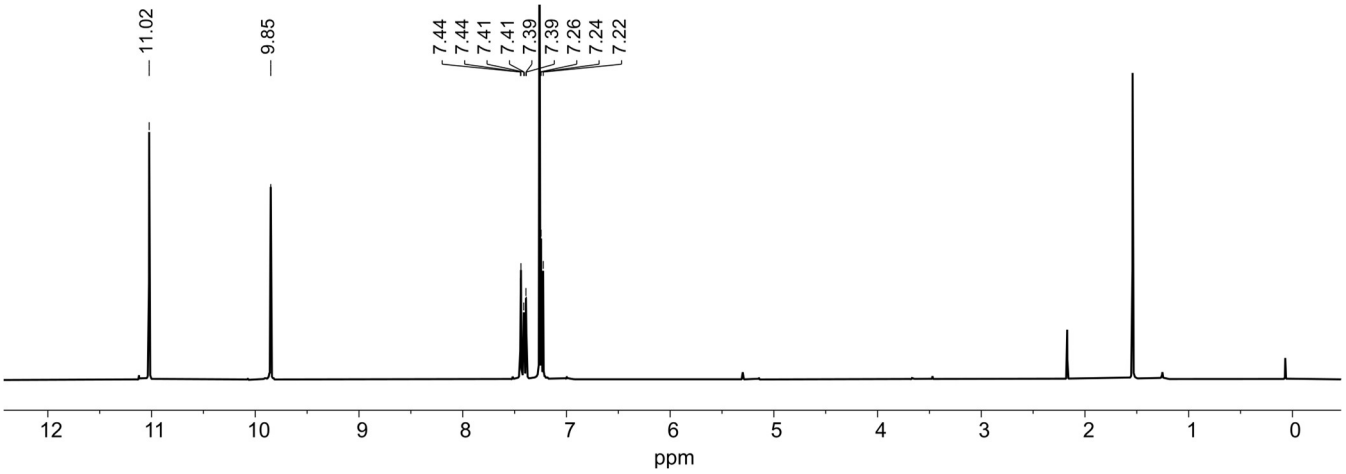

Fig. S1.^{1}H NMR (400 MHz, C*D*Cl$_3$, 25 ºC) spectrum of **1**.

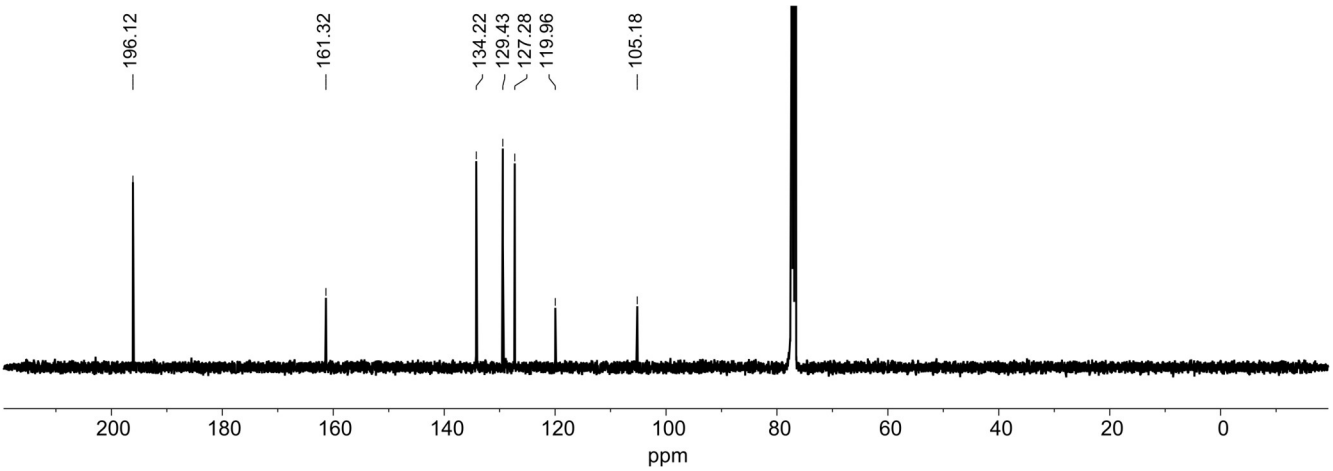

Fig. S2. ^{13}C{^{1}H} NMR (101 MHz, C*D*Cl$_3$, 25 ºC) spectrum of **1**.

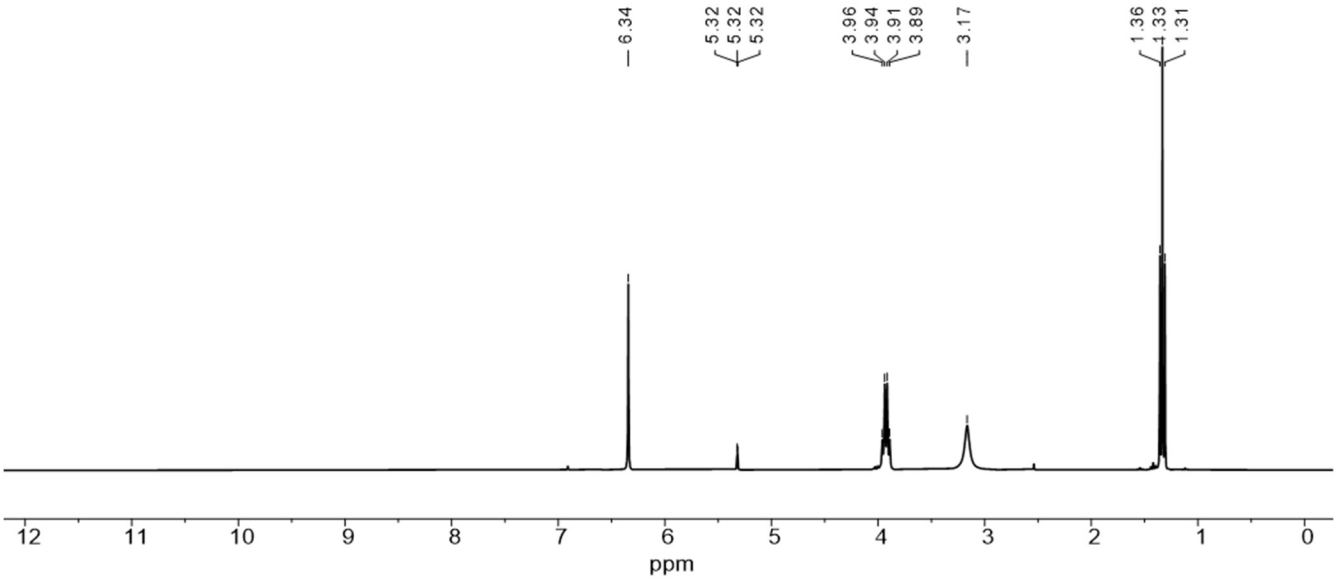

Fig. S3. ^{1}H NMR (400 MHz, DCM-d_2, 25 ºC) spectrum of **2b**.

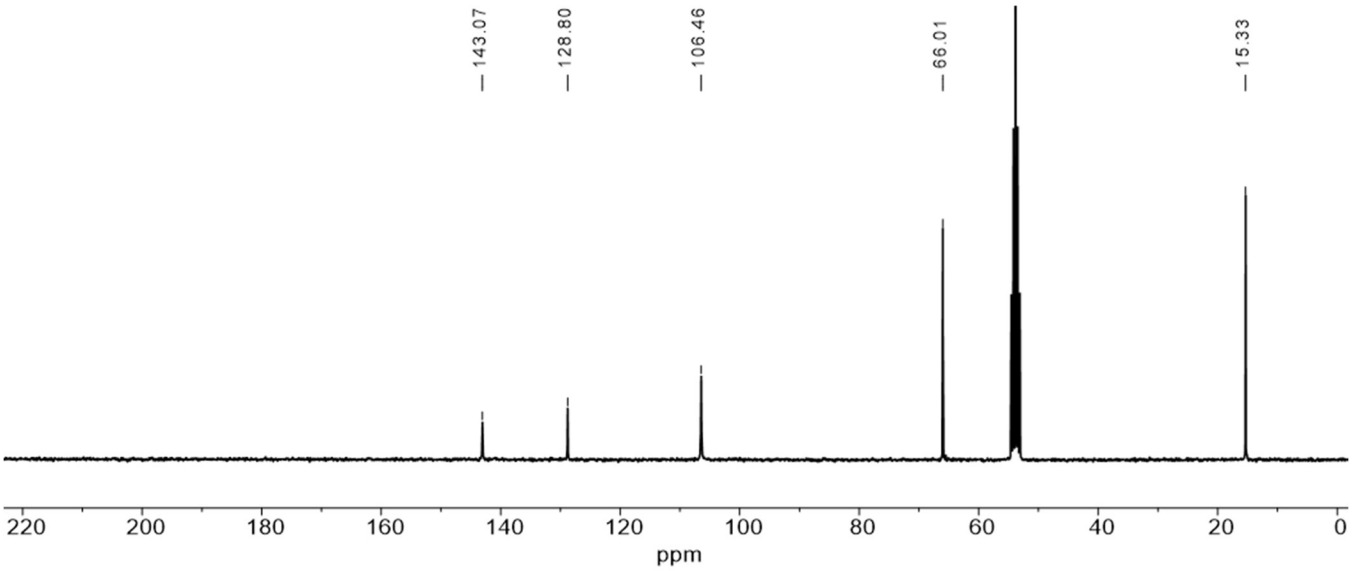

Fig. S4. ^{13}C{^{1}H} NMR (101 MHz, DCM-d_2, 25 ºC) spectrum of **2b**.

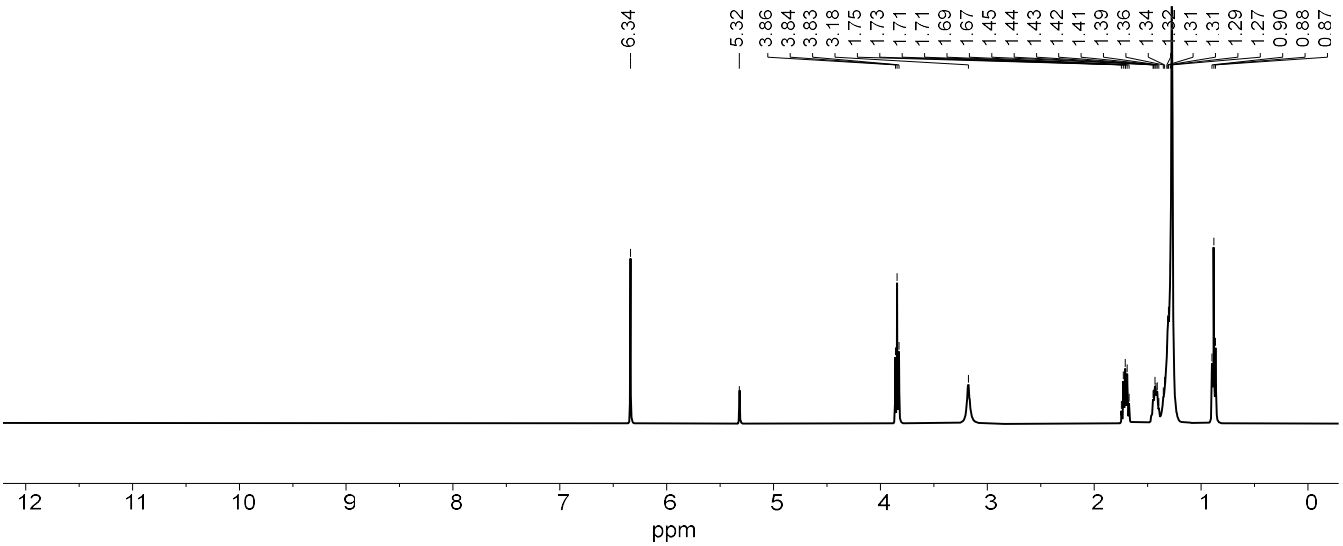

Fig. S5. ^{1}H NMR (400 MHz, DCM-d_2, 25 ºC) spectrum of **2c**.

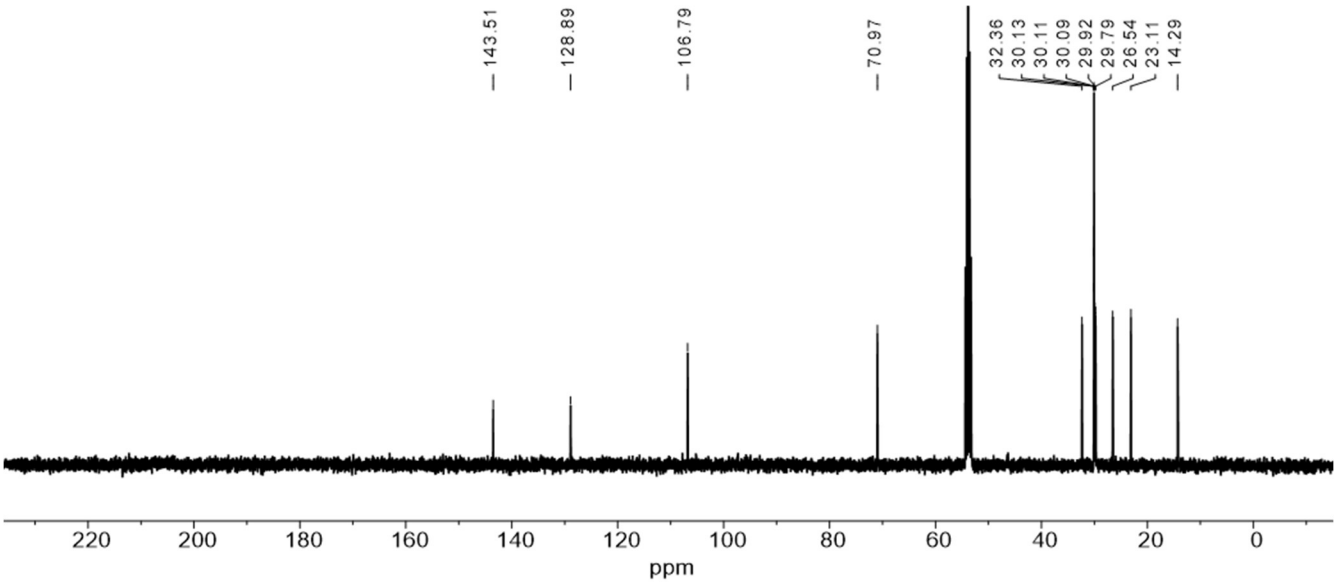

Fig. S6. ^{13}C{^{1}H} NMR (101 MHz, DCM-d_2, 25 ºC) spectrum of **2c**.

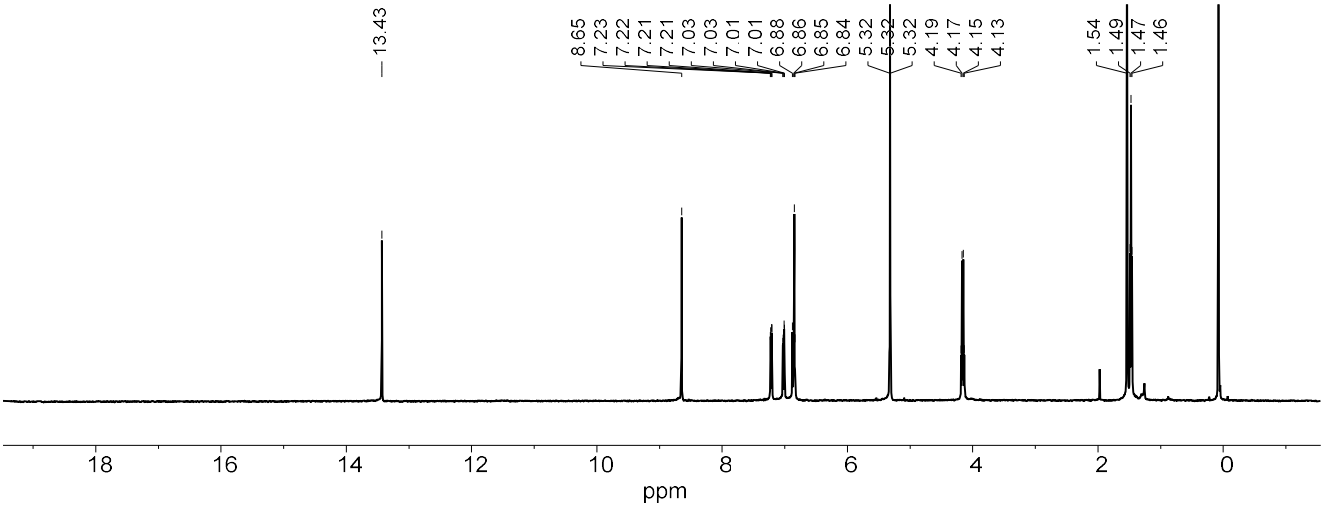

Fig. S7. ^{1}H NMR (400 MHz, DCM-d_2, 25 ºC) spectrum of **3b**.

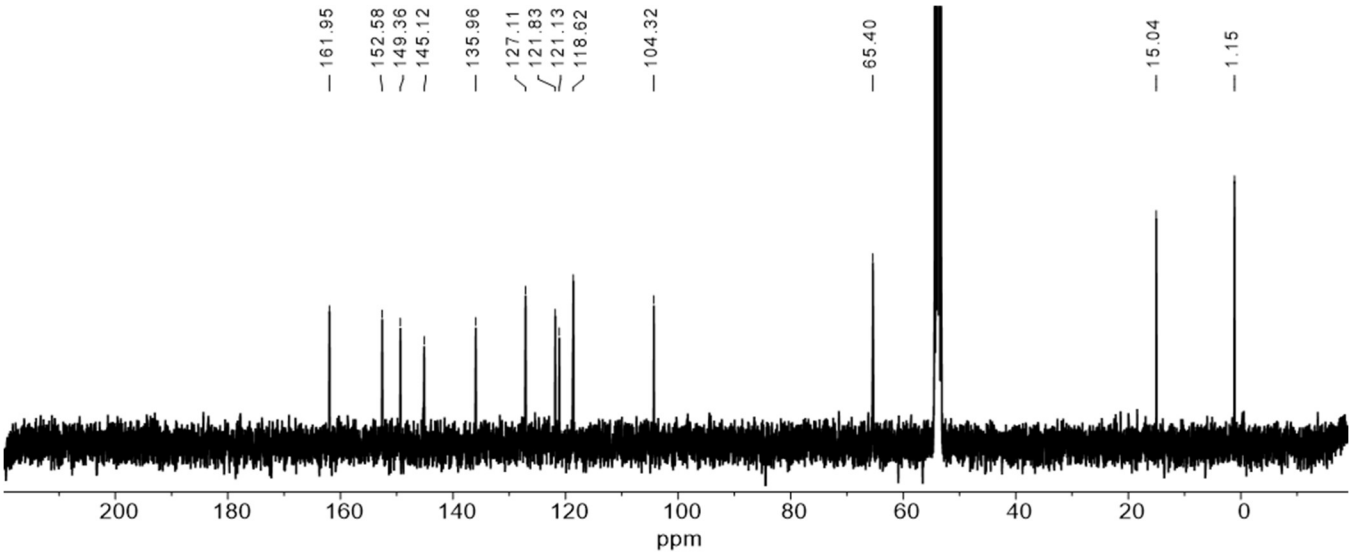

Fig. S8. $^{13}C\{^{1}H\}$ NMR (101 MHz, DCM-d_2, 25 ºC) spectrum of **3b**.

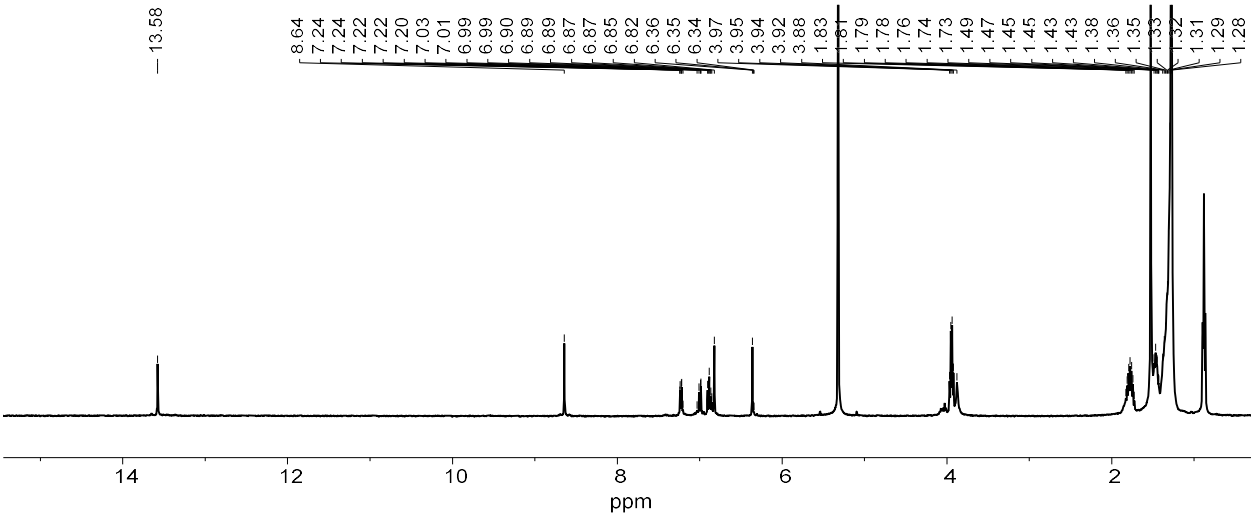

Fig. S9. ^{1}H NMR (400 MHz, DCM-d_2, 25 ºC) spectrum of **3c**.

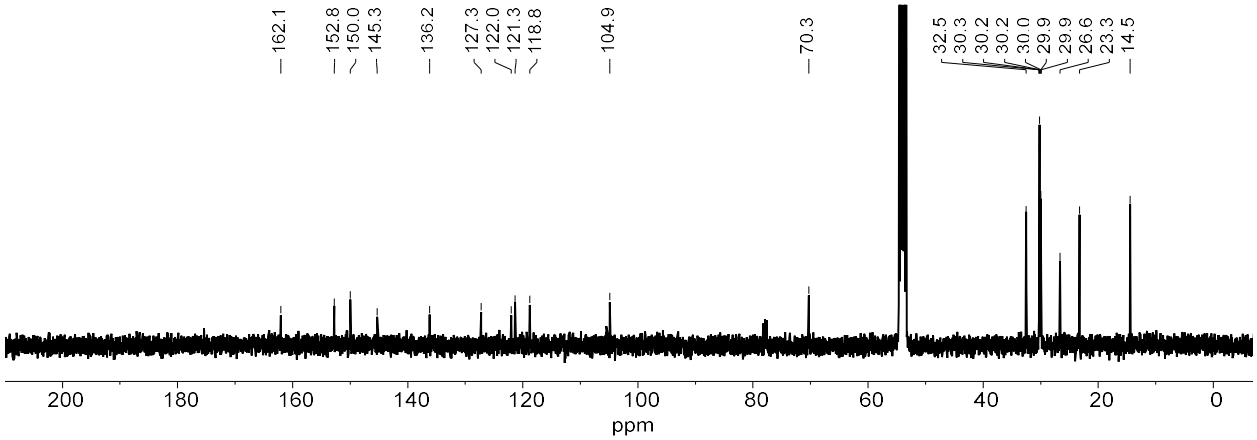

Fig. S10.$^{13}C\{^{1}H\}$ NMR (101 MHz, DCM-d_2, 25 ºC) spectrum of **3c**.

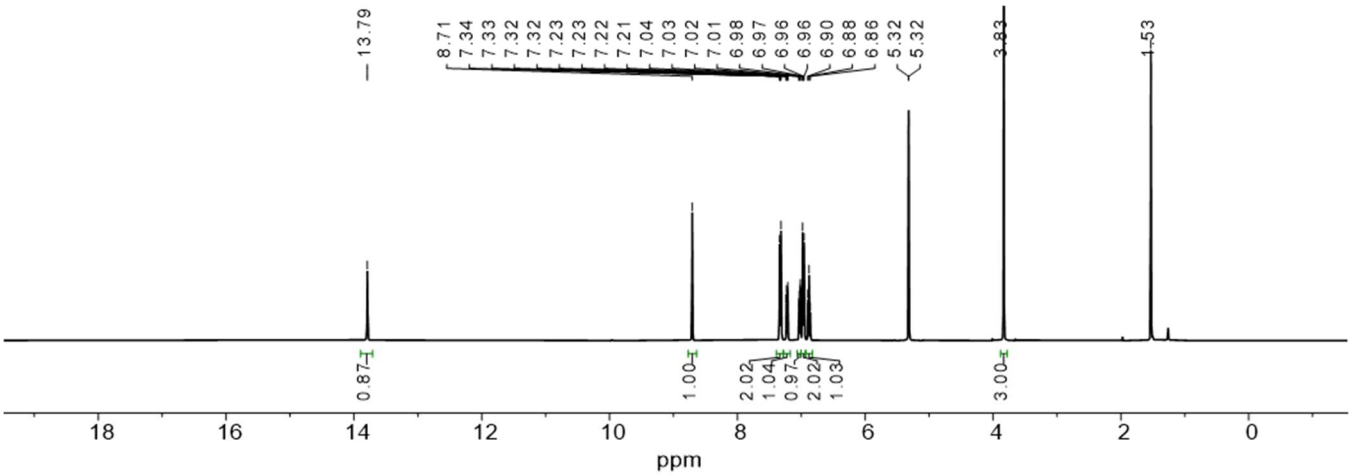

Fig. S11. ^{1}H NMR (400 MHz, DCM-d_2, 25 ºC) spectrum of **4**.

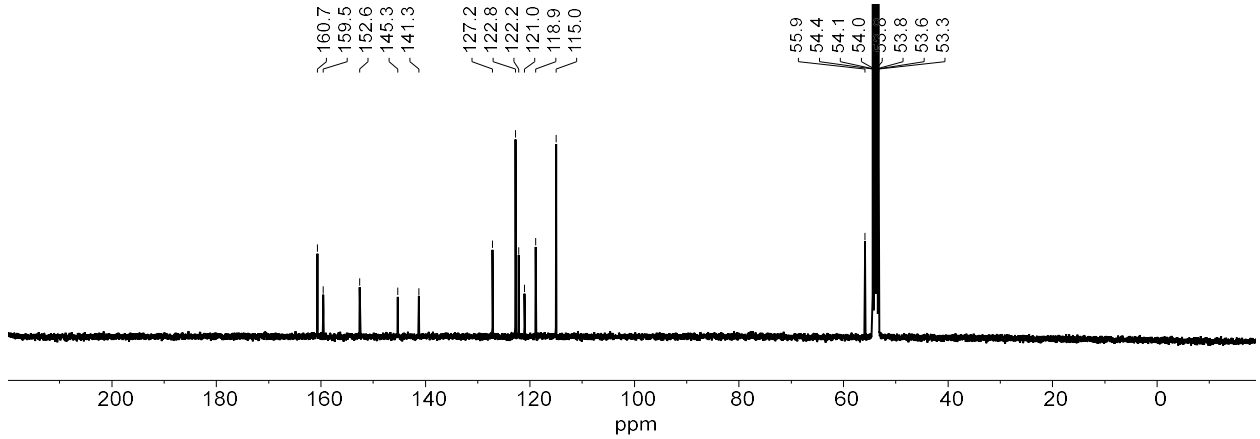

Fig. S12. ^{13}C{^{1}H} NMR (101 MHz, DCM-d_2, 25 ºC) spectrum of **4**.

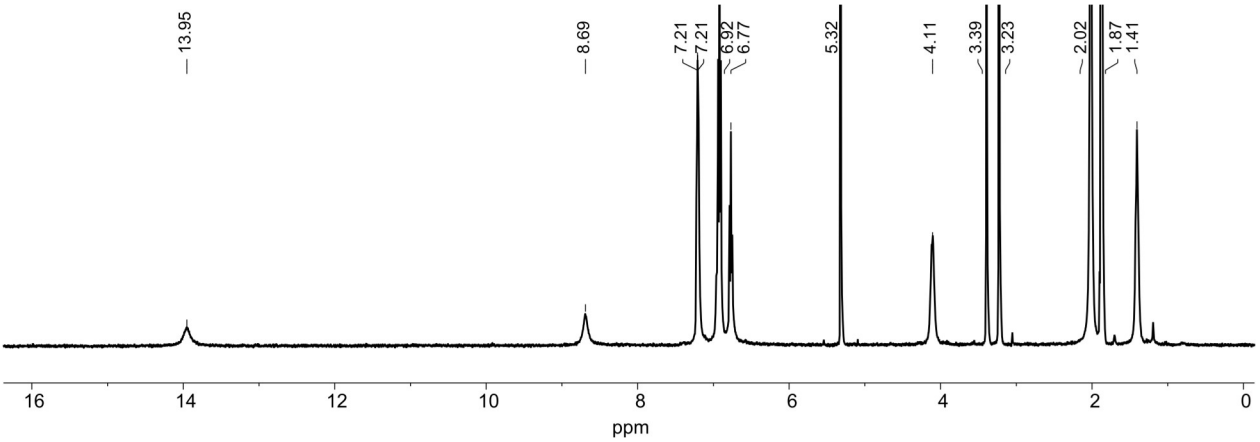

Fig. S13. ^{1}H NMR (400 MHz, DCM-d_2/MeCN-d_3, 25 ºC) spectrum for **3b+Li^{+}**.

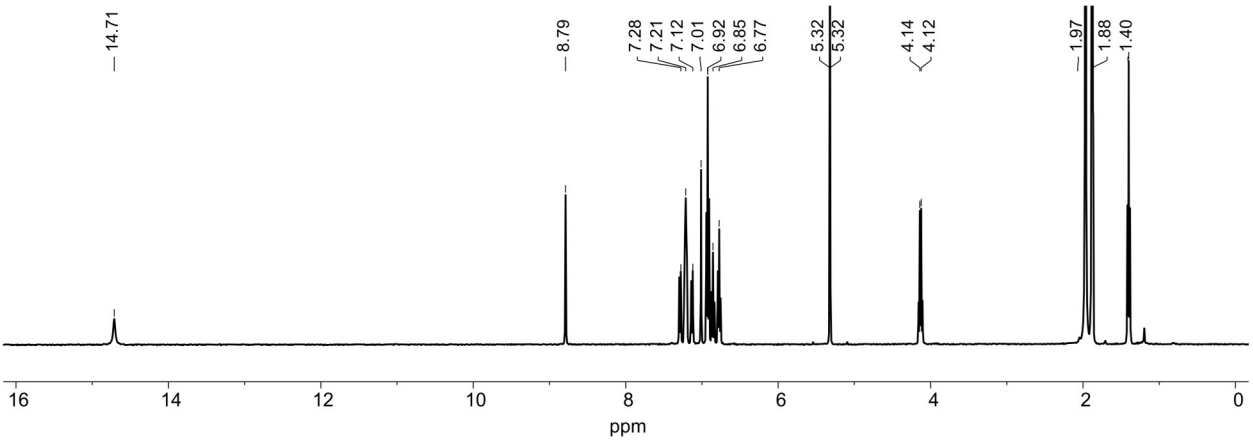

Fig. S14. ^{1}H NMR (400 MHz, DCM-d_2/MeCN-d_3, 25 ºC) spectrum for **3b+Na^{+}**.

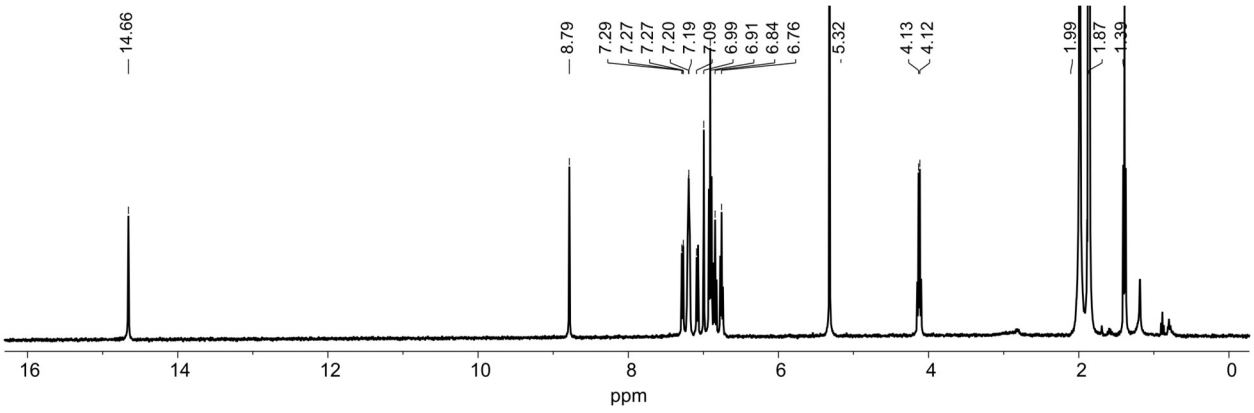

Fig. S15. ^{1}H NMR (400 MHz, DCM-d_2/MeCN-d_3, 25 ºC) spectrum for **3b+K^{+}**.

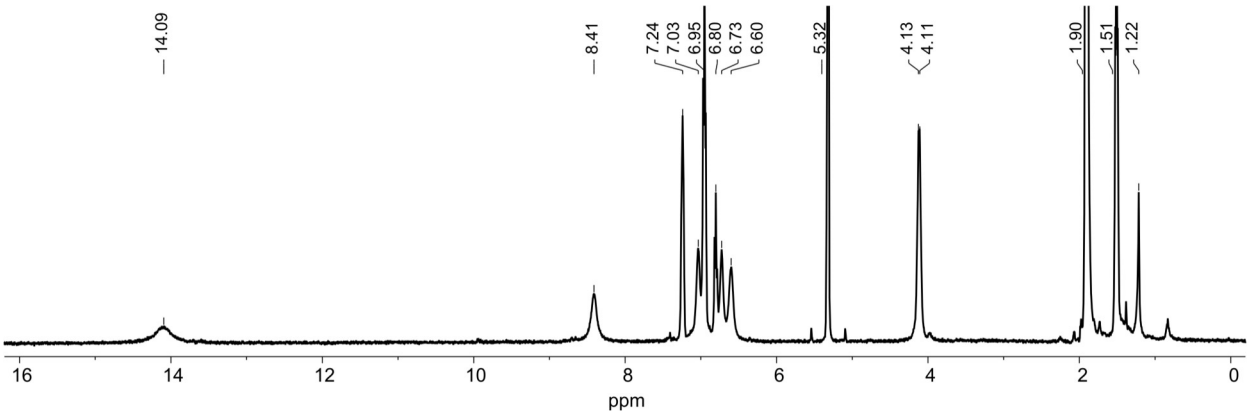

Fig. S16. ^{1}H NMR (400 MHz, DCM-d_2/MeCN-d_3, 25 ºC) spectrum for **3b+Rb^{+}**.

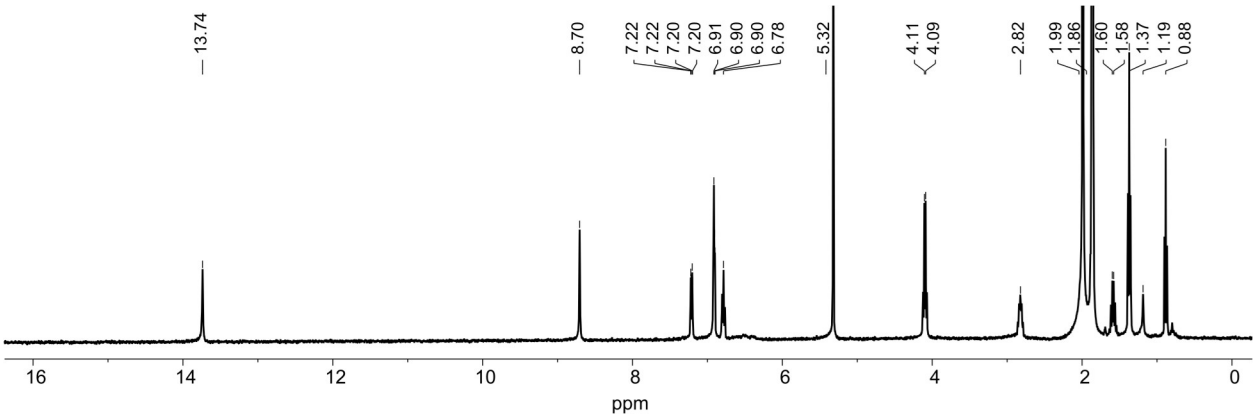

Fig. S17. ^{1}H NMR (400 MHz, DCM-d_2/MeCN-d_3, 25 ºC) spectrum for **3b+DPA^{+}**.

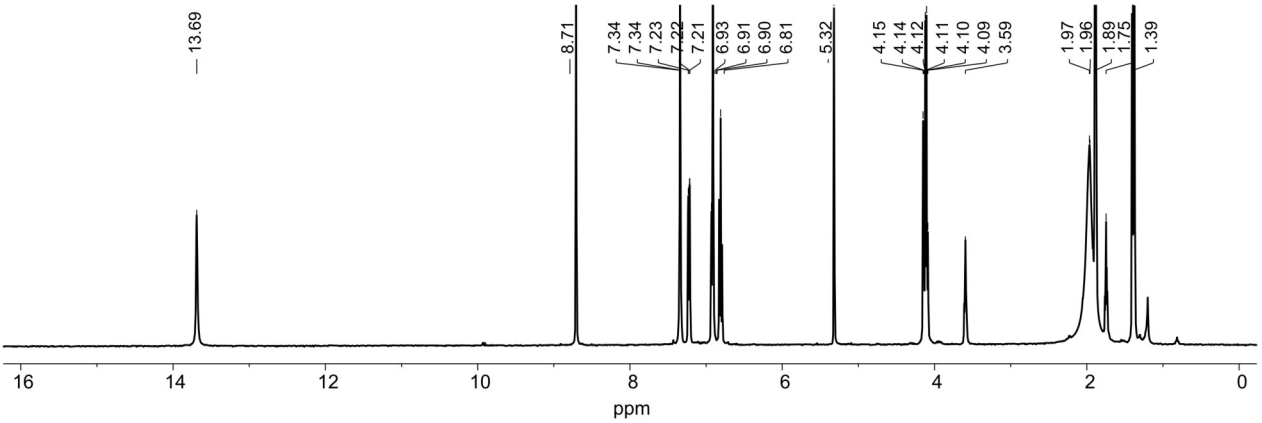

Fig. S18. ^{1}H NMR (400 MHz, DCM-d_2/MeCN-d_3, 25 ºC) spectrum for **3b+DBA^{+}**.

DOSY NMR spectra

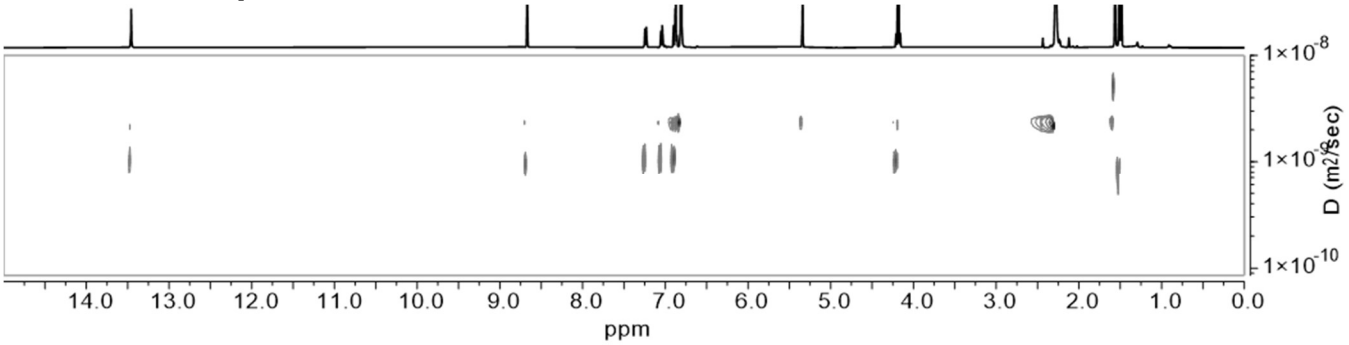

Fig. S19. DOSY NMR (400 MHz, DCM-d_2/MeCN-d_3, 25 ºC) spectrum for **3b** with mesitylene.

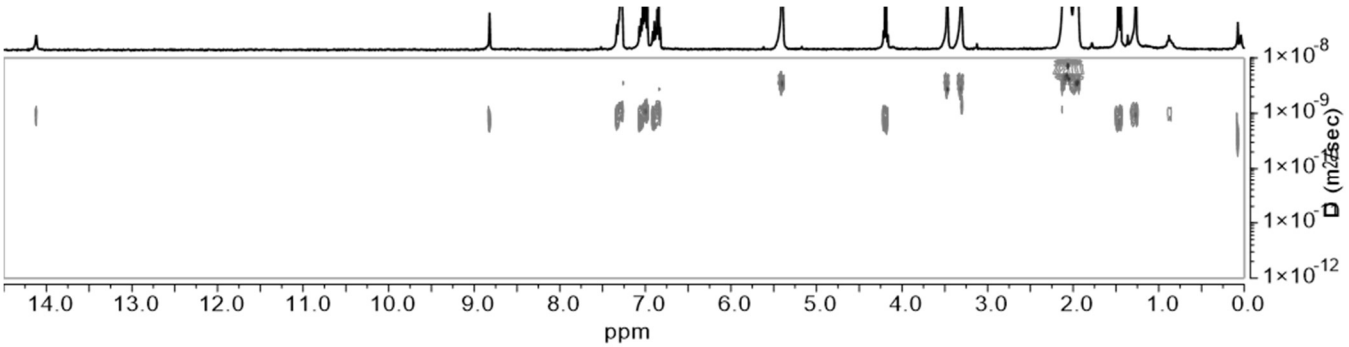

Fig. S20. DOSY NMR (400 MHz, DCM-d_2/MeCN-d_3, 25 ºC) spectrum for **3b+Li^{+}**.

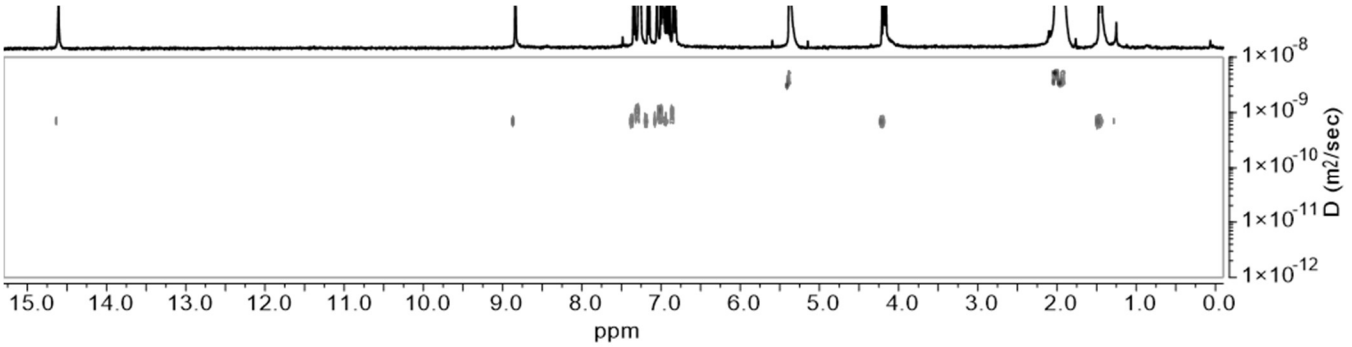

Fig. S21. DOSY NMR (400 MHz, DCM-d_2/MeCN-d_3, 25 ºC) spectrum for **3b+Na$^+$**.

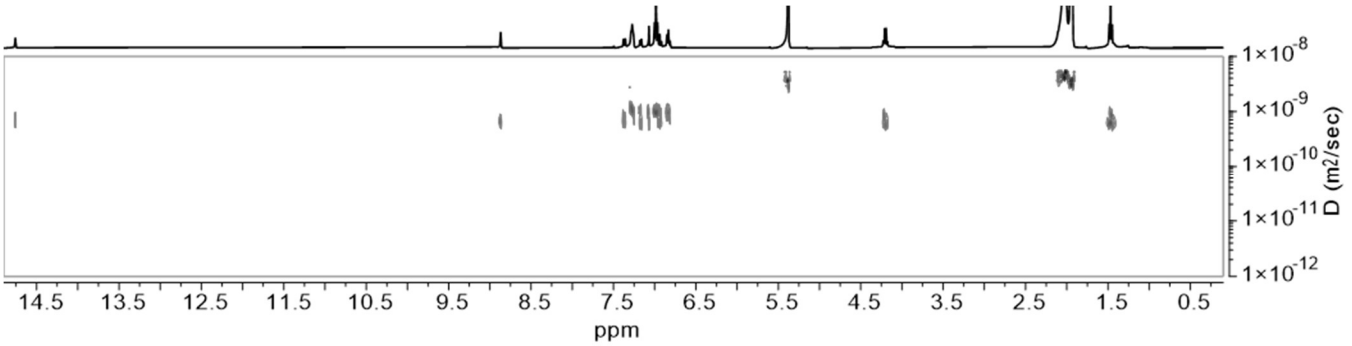

Fig. S22. DOSY NMR (400 MHz, DCM-d_2/MeCN-d_3, 25 ºC) spectrum for **3b+K$^+$**.

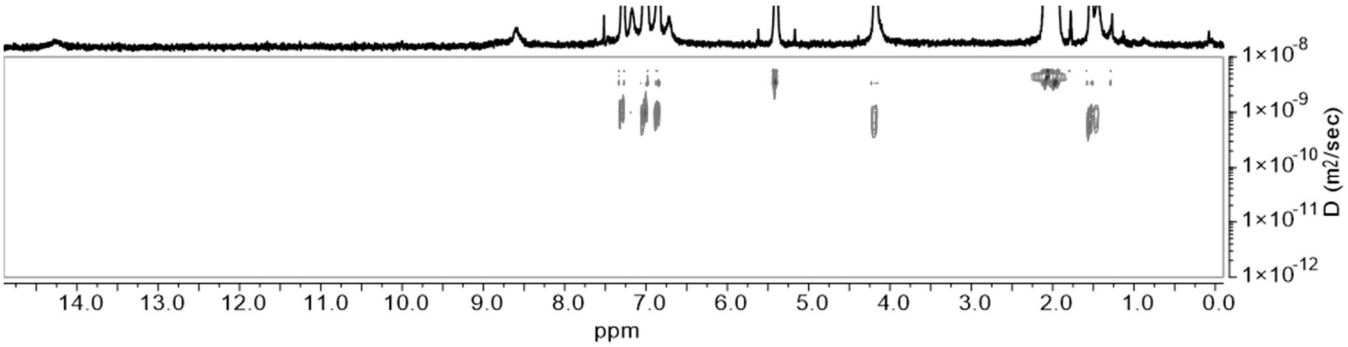

Fig. S23. DOSY NMR (400 MHz, DCM-d_2/MeCN-d_3, 25 ºC) spectrum for **3b+Rb$^+$**.

Other spectra

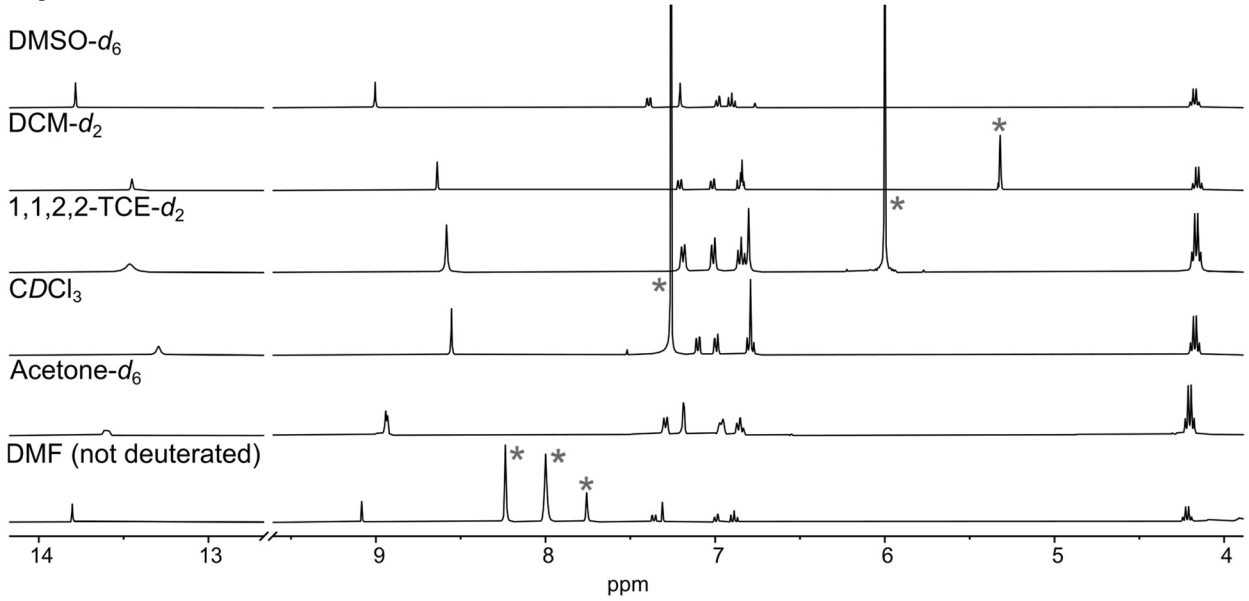

Fig. S24. Stacked partial ^{1}H NMR (400 MHz, 25 ºC) for **3b** in several different solvents. * = solvent residual peak(s).

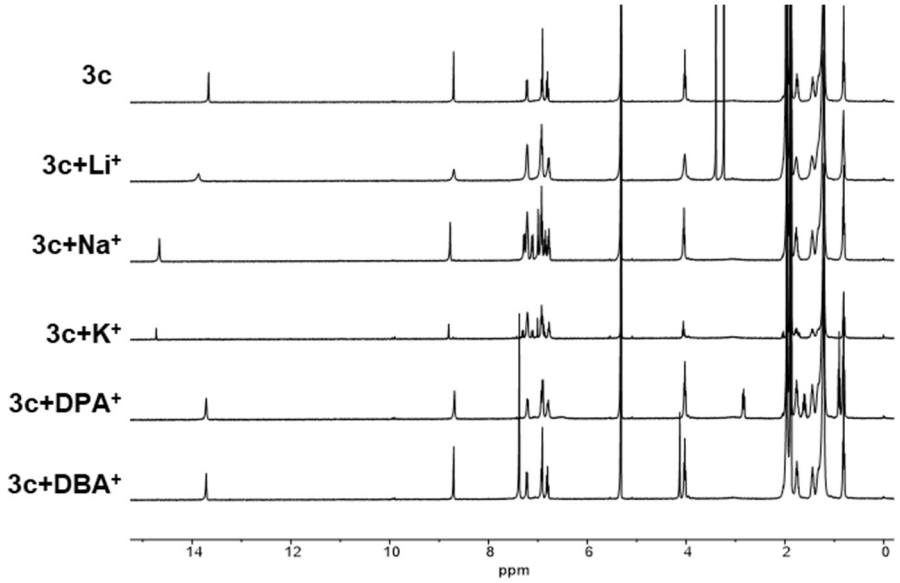

Fig. S25. Stacked ^{1}H NMR (400 MHz, DCM-d_2/MeCN-d_3, 25 ºC) for **3c** with various guest cations (1:1) ratio.

NOTE: all samples had significant precipitation once the guest was added, even at low concentrations (*ca.* 1 mM).

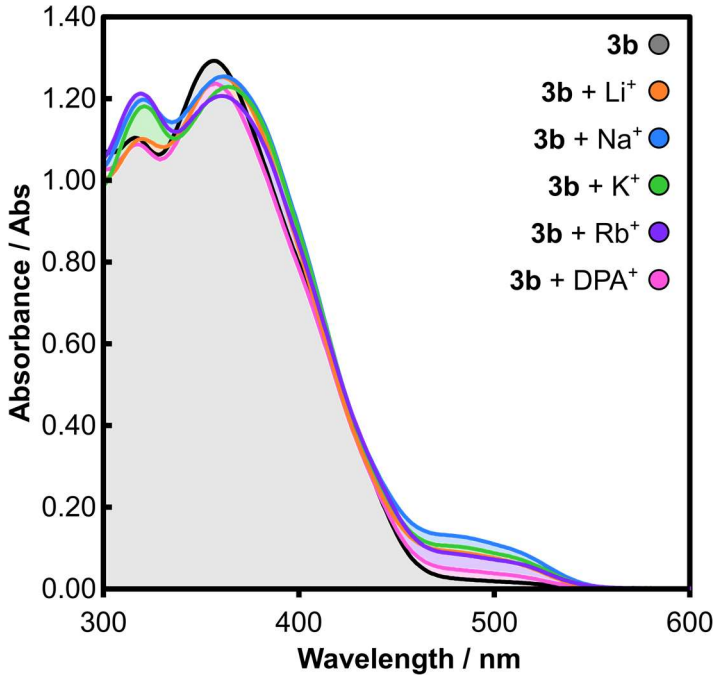

Fig. S26. Stacked UV-vis spectra for **3b** with various guests.

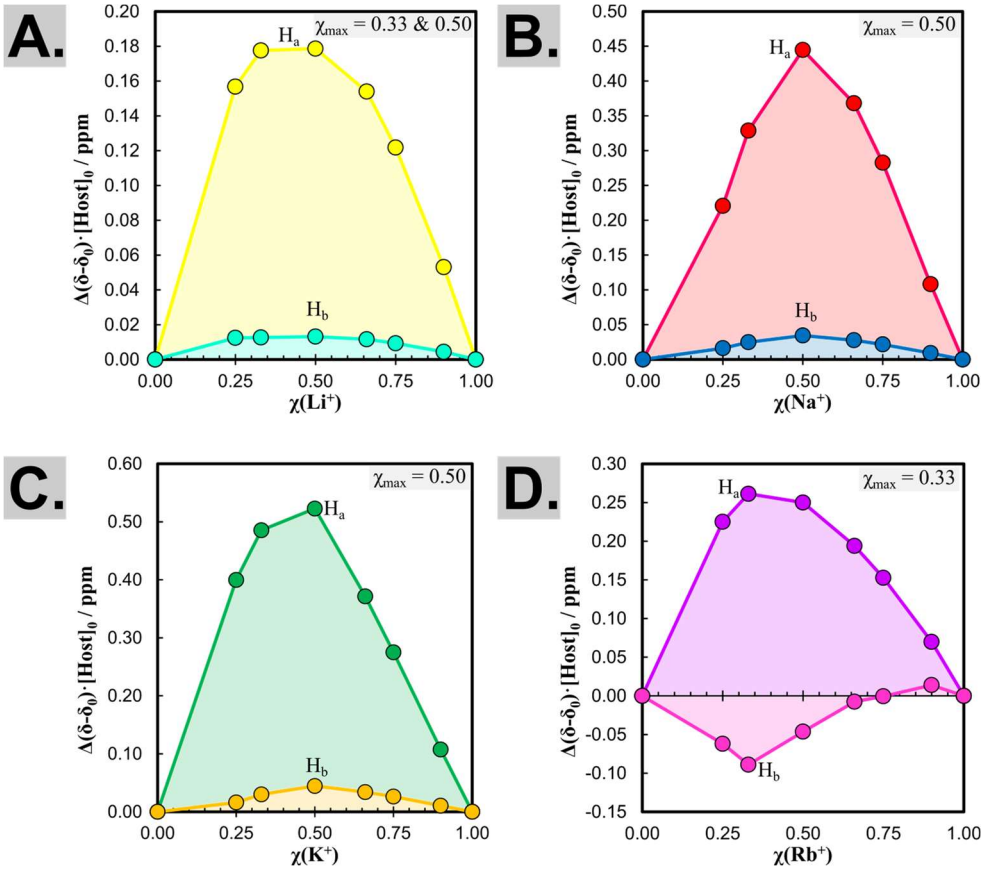

Fig. S27. Modified ^{1}H NMR Job plots ($\Delta\delta$·[Host]$_0$ plotted against mole fraction (χ) of guest to host) for A) **3b+Li$^+$**, B) **3b+Na$^+$**, C) **3b+K$^+$**, and D) **3b+Rb$^+$**. (Total host+guest concentration kept at 1 mM). Data for both H_a and H_b are given.

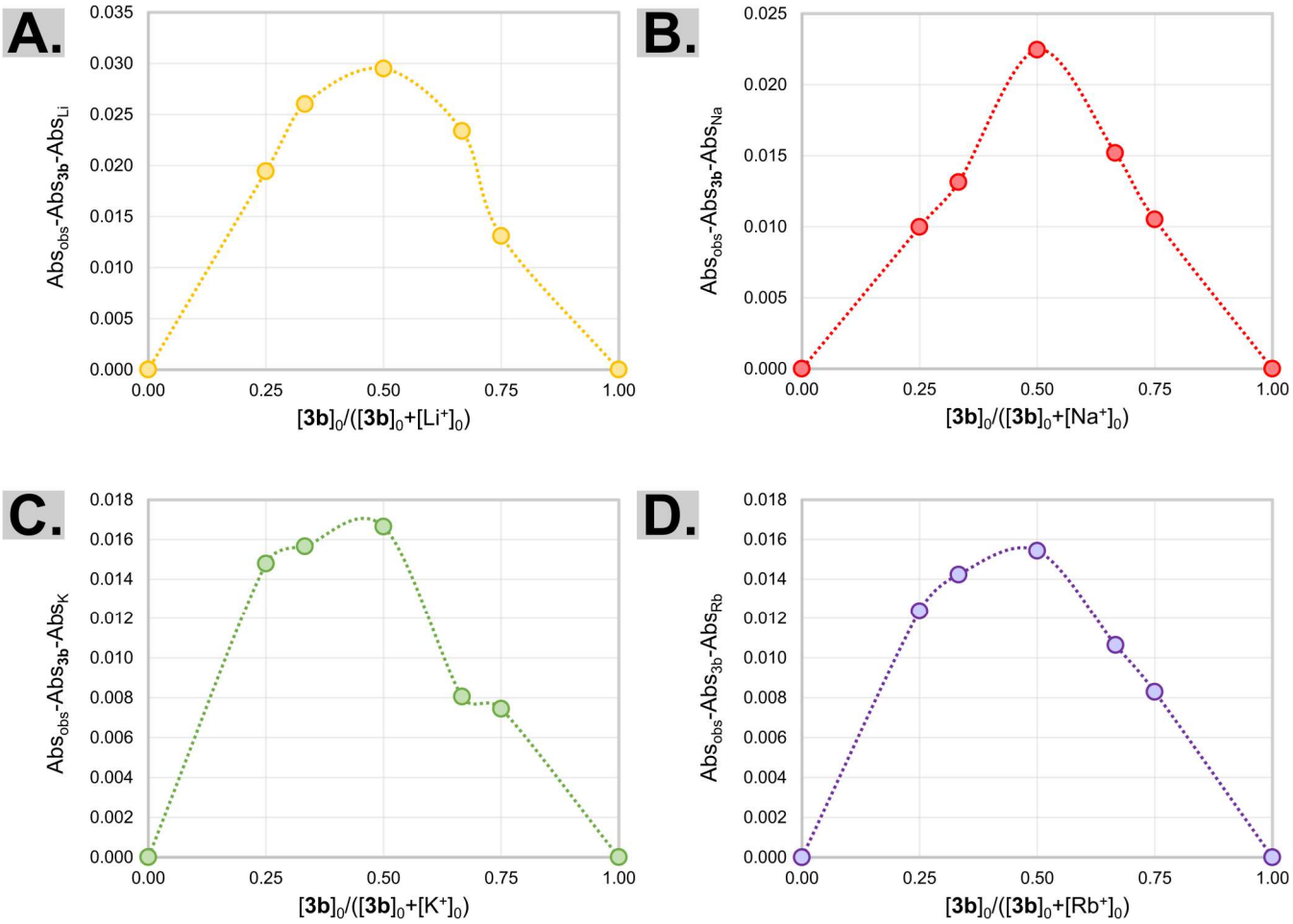

Fig. S28. Modified UV-vis Job plots for A) **3b+Li$^+$**, B) **3b+Na$^+$**, C) **3b+K$^+$**, and D) **3b+Rb$^+$**. (Total host+guest concentration kept at 2 x 10^{-5} M). All Job plots show a maxima at χ = 0.5, implying a 1:1 binding stoichiometry.

MS Data for 3b and corresponding host-guest complexes

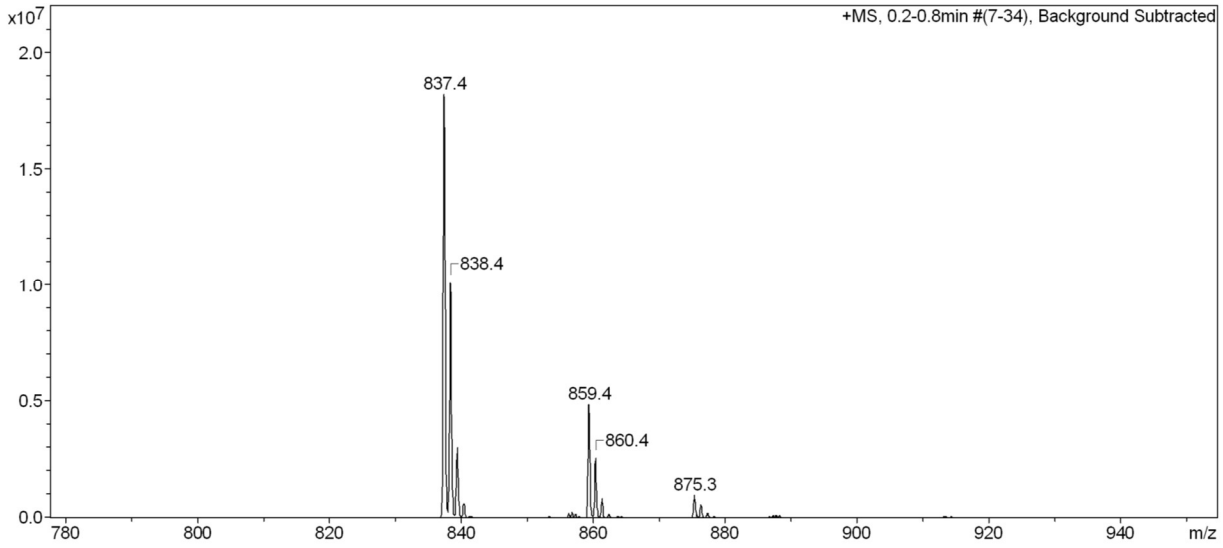

Fig. S29. LRMS (ESI) mass spectrum for **3b**.

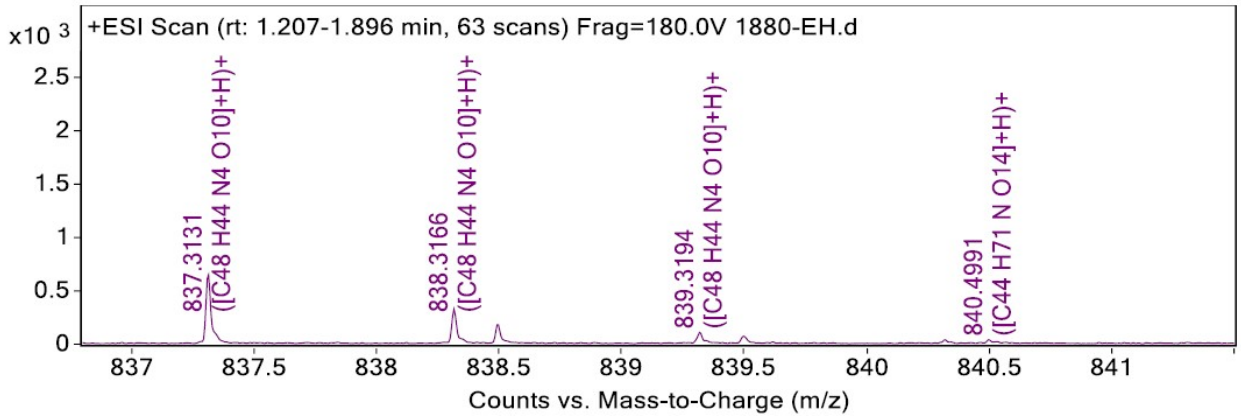

Fig. S30. HRMS (ESI) mass spectrum of **3b**.

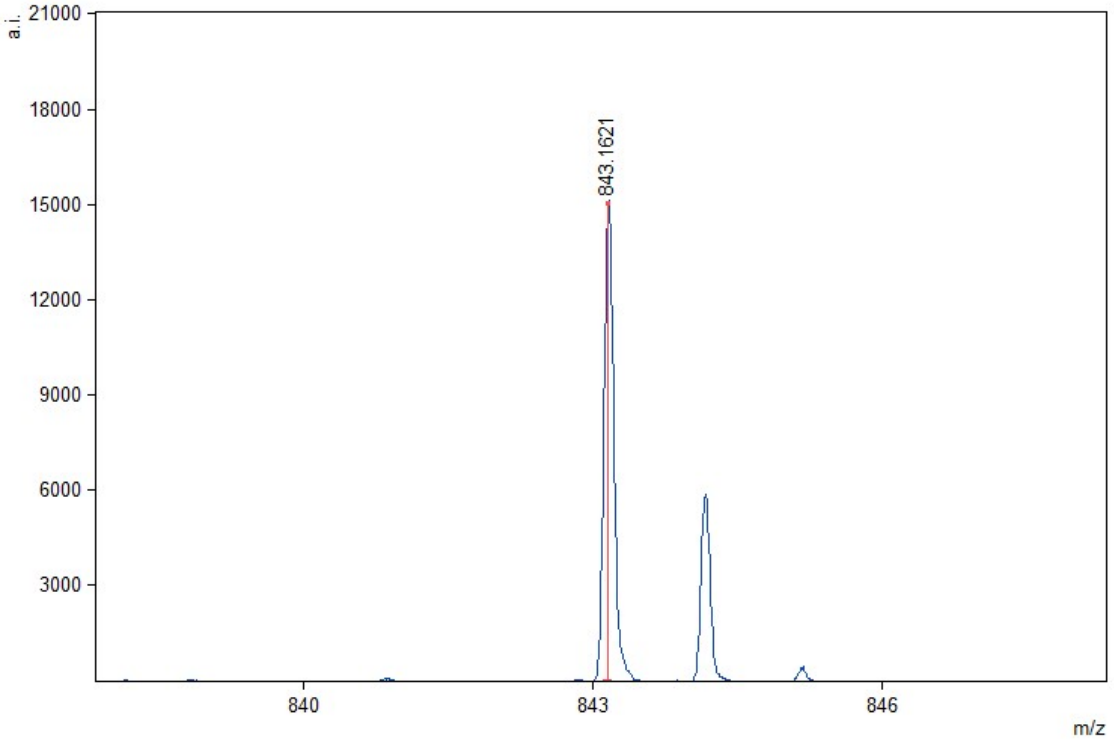

Fig. S31. LRMS (MALDI-TOF) mass spectrum for **3b+Li**$^{+}$.

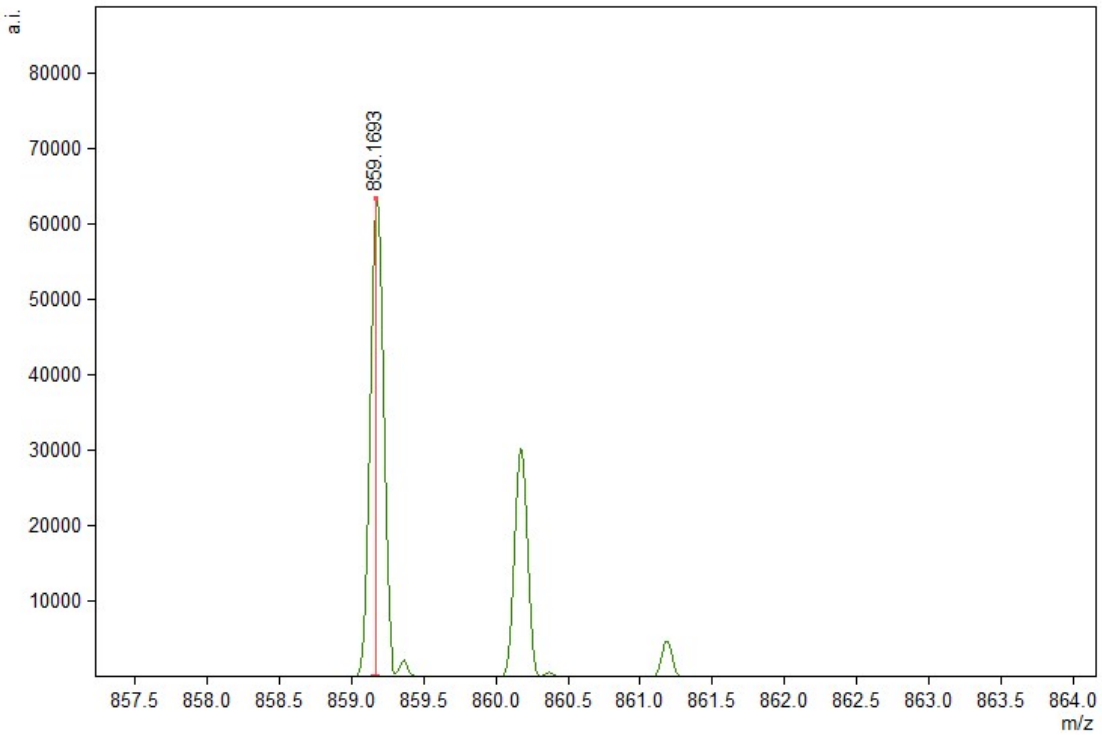

Fig. S32. LRMS (MALDI-TOF) mass spectrum for **3b+Na**$^{+}$.

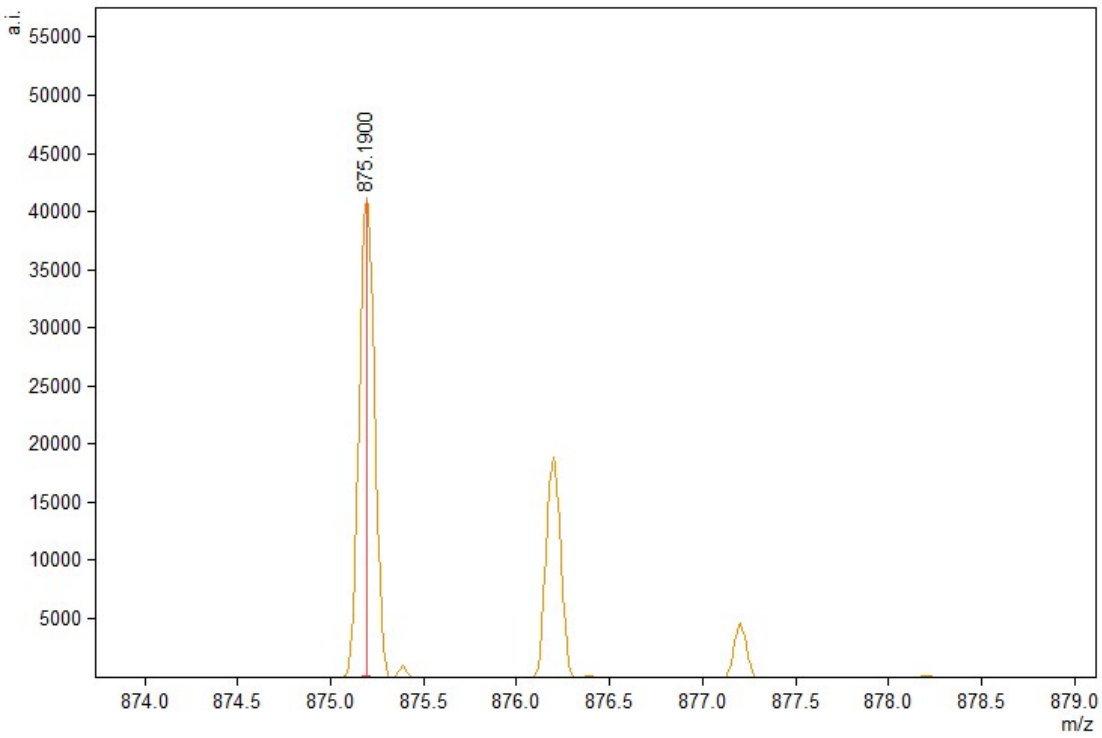

Fig. S33. LRMS (MALDI-TOF) mass spectrum for **3b+K$^+$**.

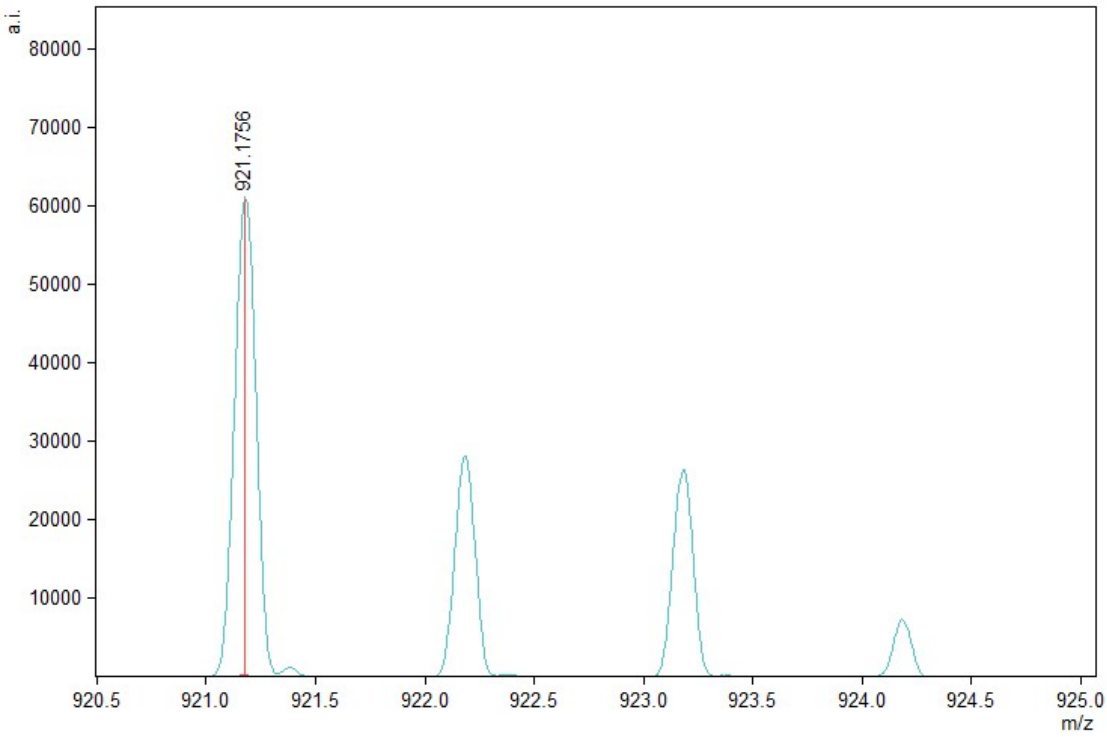

Fig. S34. LRMS (MALDI-TOF) mass spectrum for **3b+Rb$^+$**.

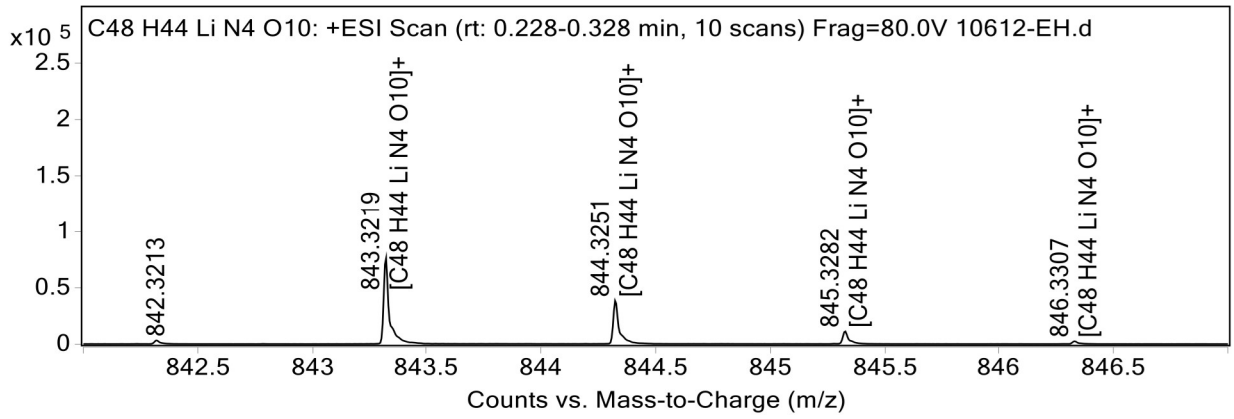

Fig. S35. HRMS (ESI) mass spectrum of **3b+Li$^+$**.

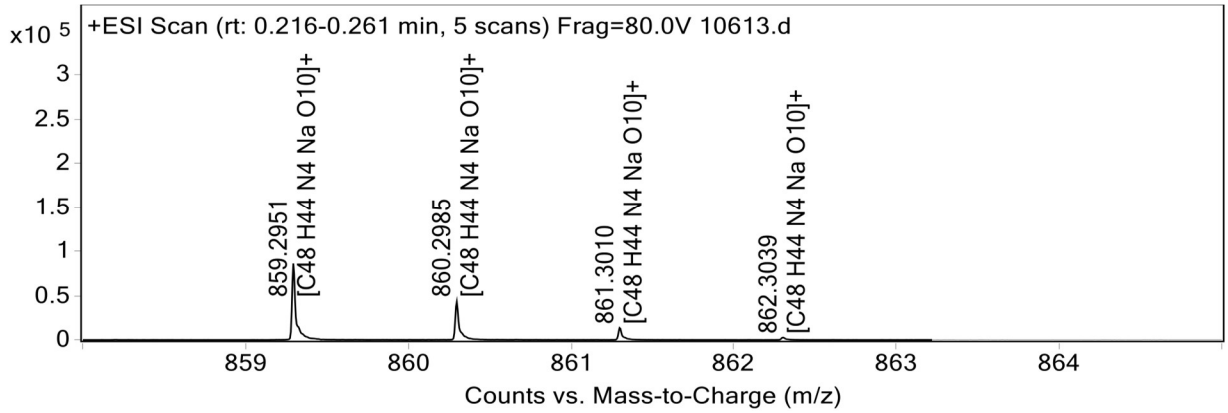

Fig. S36. HRMS (ESI) mass spectrum of **3b+Na$^+$**.

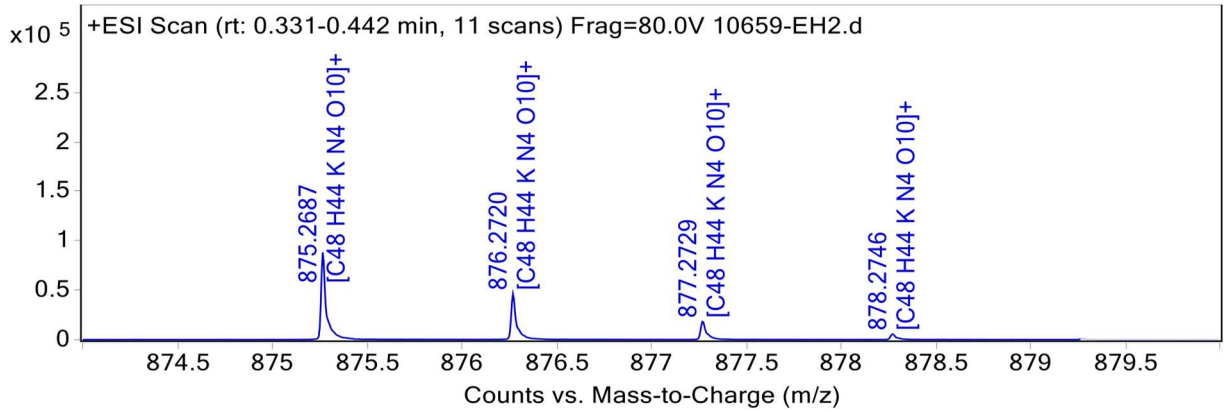

Fig. S37. HRMS (ESI) mass spectrum of **3b+K$^+$**.

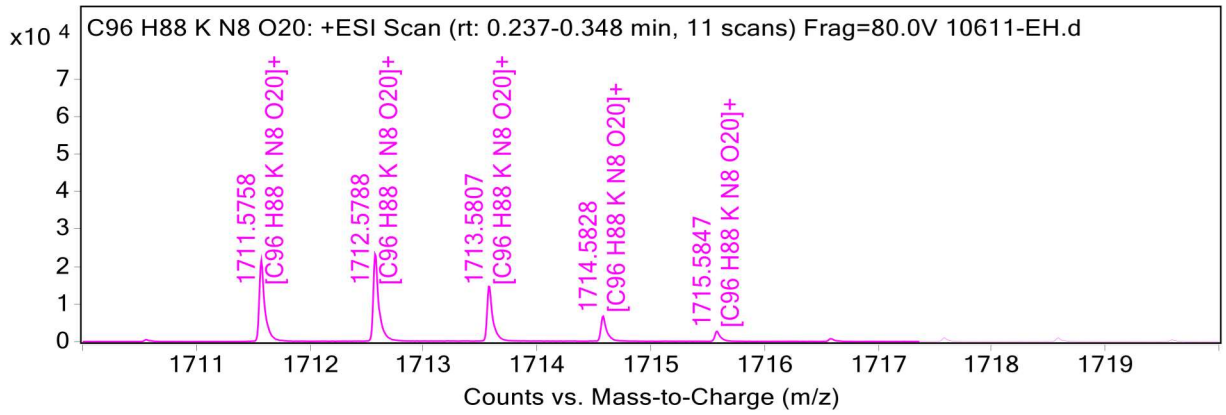

Fig. S38. HRMS (ESI) mass spectrum of $(\mathbf{3b})_2\mathbf{+K^+}$.

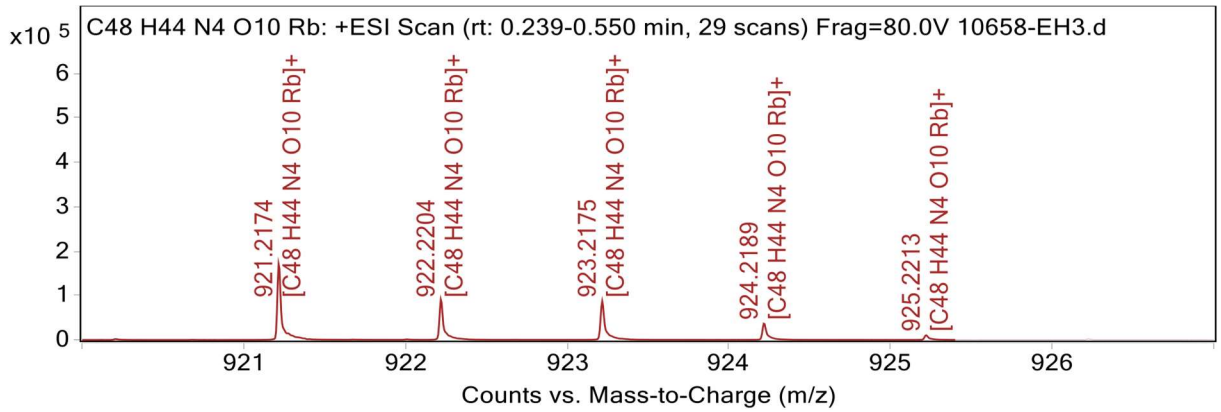

Fig. S39. HRMS (ESI) mass spectrum of $\mathbf{3b+Rb^+}$.

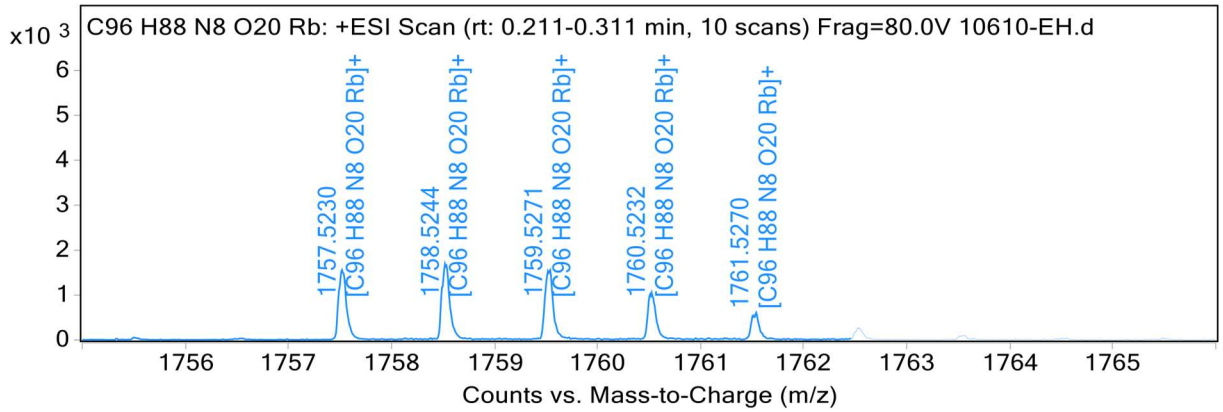

Fig. S40. HRMS (ESI) mass spectrum of $(\mathbf{3b})_2\mathbf{+Rb^+}$.

Single crystal X-ray diffraction discussion and refinement

Compound $3b_1$

Crystals were grown via slow evaporation of a solution of **3b** in DCM. Weakly diffracting crystals were obtained, so data could only be collected to a resolution of 0.93 Å using Cu Kα radiation.

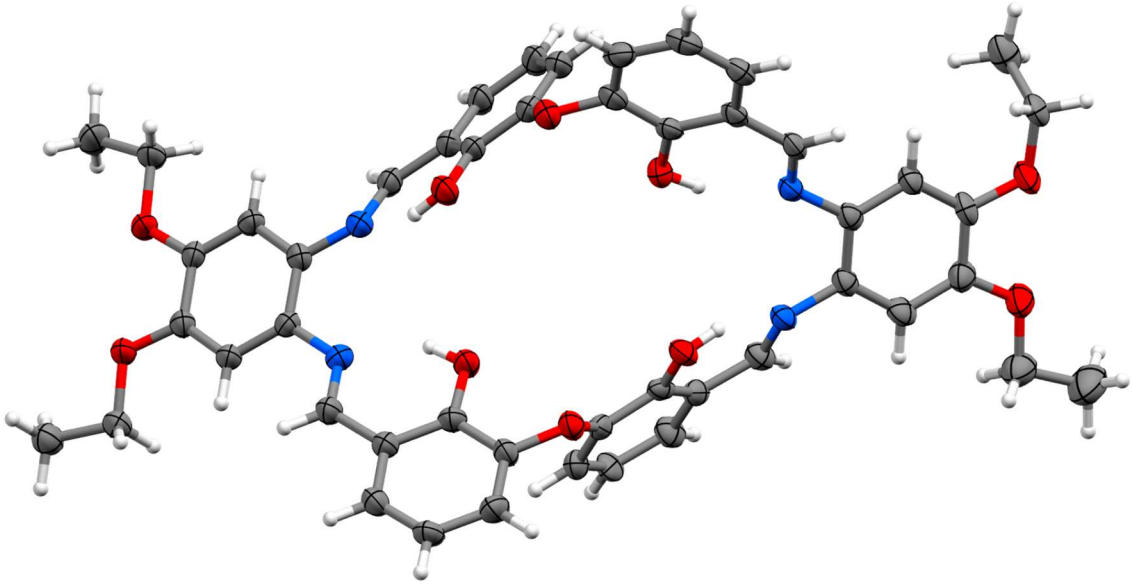

Fig. S41. Thermal-ellipsoid plot for $\mathbf{3b_1}$.

Compound $3b\cdot(MeCN)_2$

Crystals were grown via slow evaporation of a solution of **1** and **2b** in MeCN under an atmosphere of Ar. A molecule of MeCN was disordered and modelled in parts.

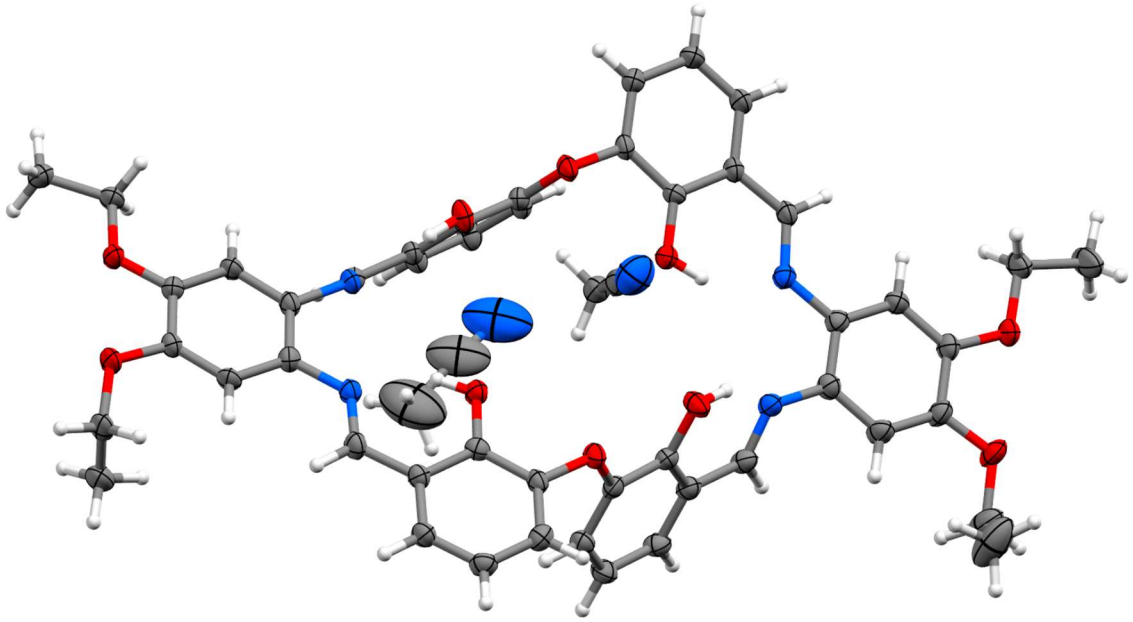

Fig. S42. Thermal-ellipsoid plot for $\mathbf{3b}\cdot(MeCN)_2$.

Compound $3b_4$

Crystals were grown via slow evaporation of a solution of **3b** in DCM and MeCN in the dark. Weakly diffracting crystals were obtained, so data could only be collected to a resolution of 0.93 Å. This dataset had lots of disordered solvent, which was removed using several PLATON/SQUEEZE cycles. A heavily disordered salicylimine fragment was modelled in parts.

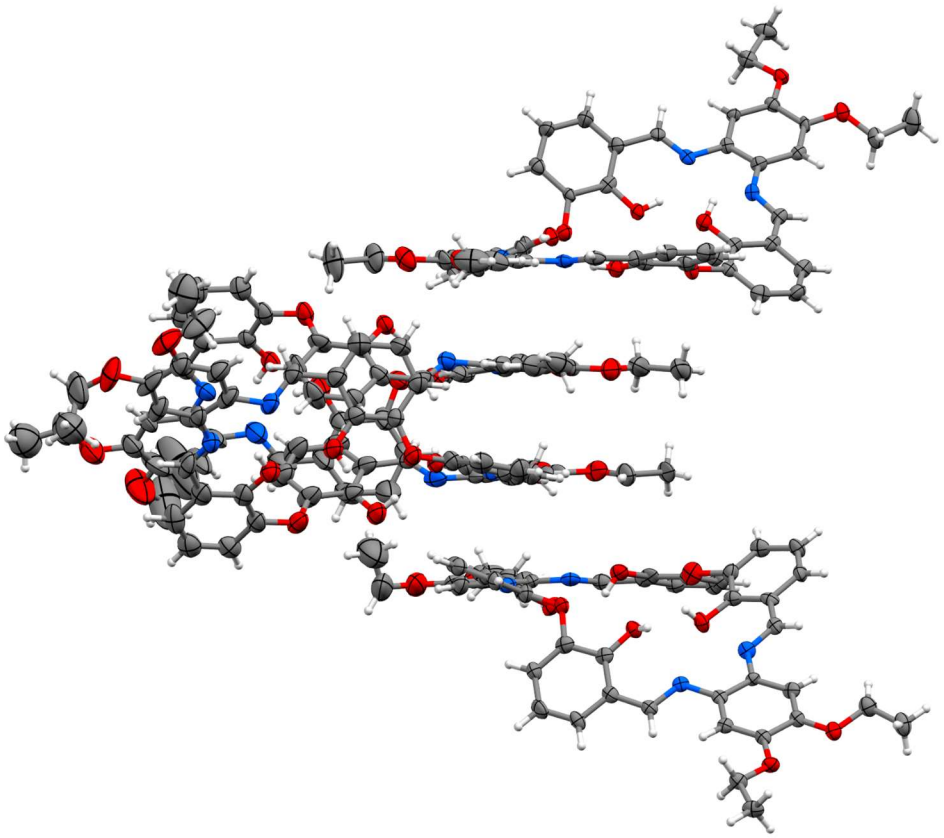

Fig. S43. Thermal-ellipsoid plot for $\mathbf{3b_4}$.

Compound 1

Crystals were grown via slow evaporation of a solution of **1** in DCM at -10 ºC. The crystals were strongly diffracting, so data were collected to a resolution of 0.70 Å using Mo Kα radiation.

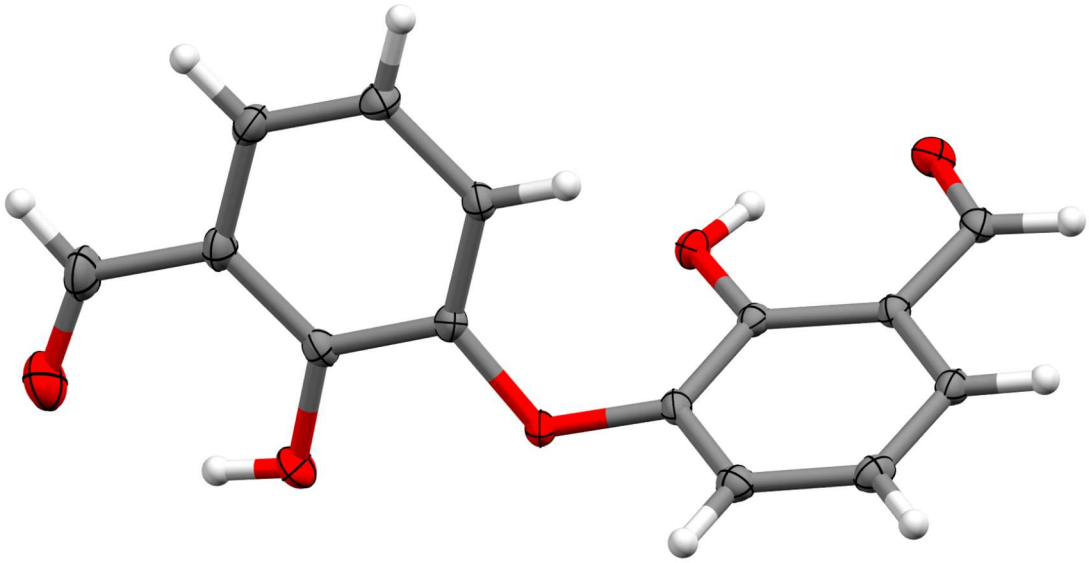

Fig. S44. Thermal-ellipsoid plot for **1**.

Compound 4

Crystals were grown via slow evaporation of a solution of **4** in DCM. The crystals were strongly diffracting, so data were collected to a resolution of 0.93 Å (Cu Kα radiation). Compound **4** crystallized as a modulated structure and was modeled using Jana2006 was used for structure solution and refinement.[8] Solving with SHEL-XT and refinement with SHEL-XL was not capable of modelling the modulated nature of the structure.[4,5]

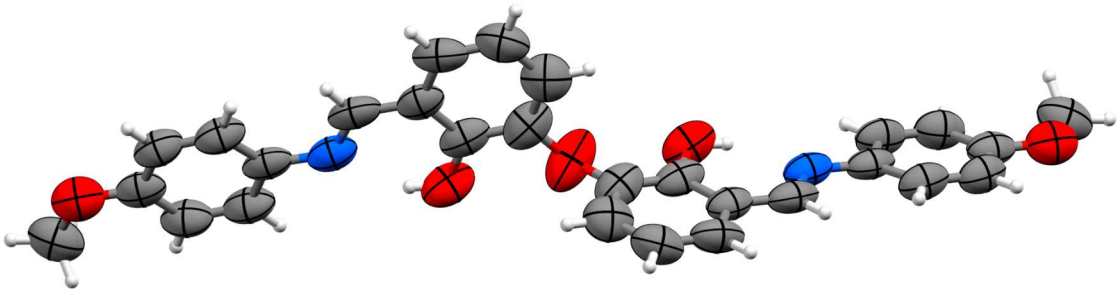

Fig. S45. Thermal-ellipsoid plot for **4**.

NMR Titration data

NMR titration of 3b with Li·BPh_4(1,2-DME)$_3$

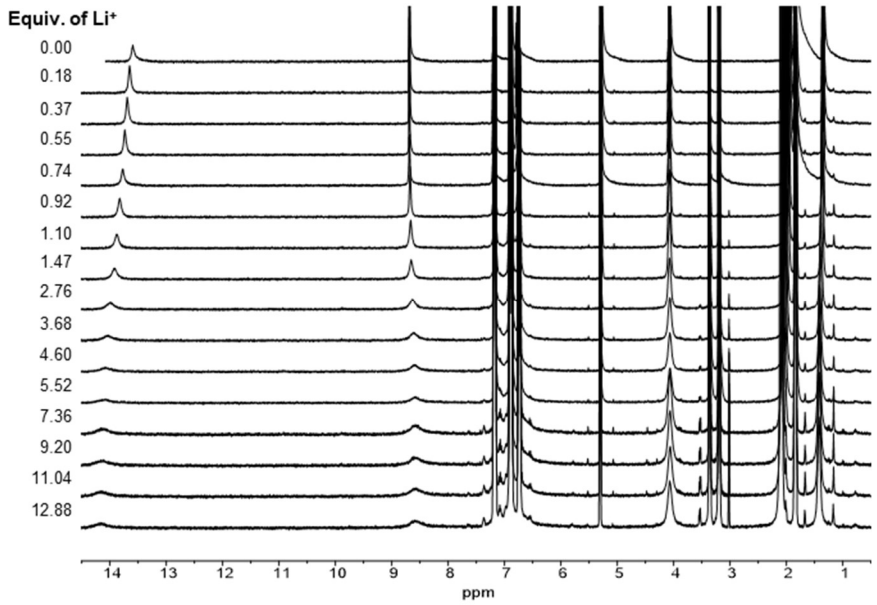

Fig. S46. Stacked ^{1}H NMR (400 MHz, DCM-d_2/MeCN-d_3, 25 ºC) spectra for the titration of **3b** with Li·BPh_4(1,2-DME)$_3$.

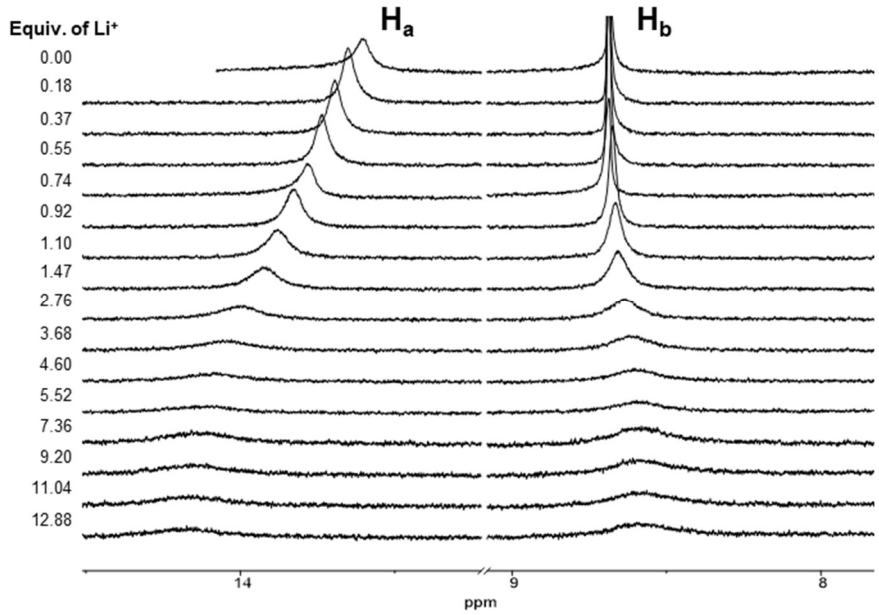

Fig. S47. Partial Stacked ^{1}H NMR (400 MHz, DCM-d_2/MeCN-d_3, 25 ºC) spectra for the titration of **3b** with Li·BPh_4(1,2-DME)$_3$ Specifically highlighting H_a and H_b.

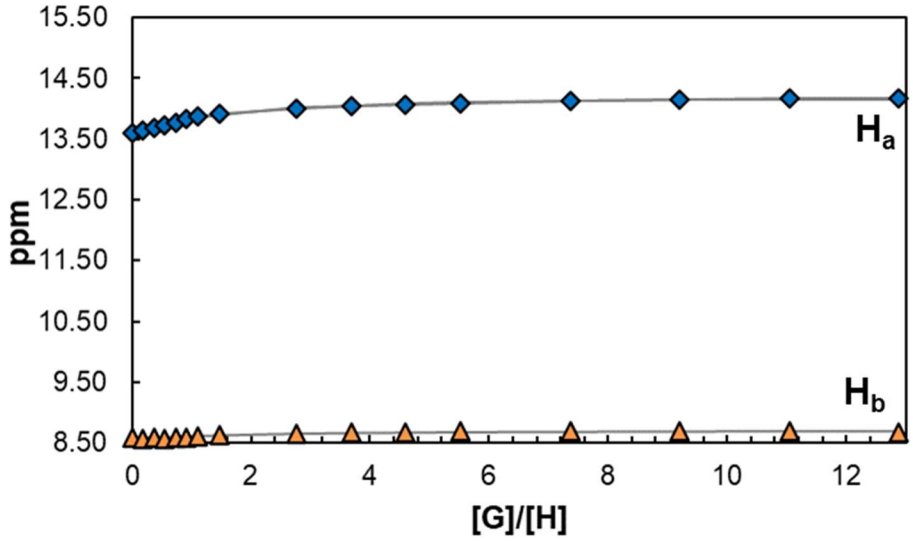

Fig. S48. ^{1}H NMR isotherms for resonances H_a and H_b obtained from the titration of **3b** with Li·BPh_4(1,2-DME)$_3$. Markers for experimental data, trend line for fit data.

NMR titration of 3b with Na·BPh$_4$

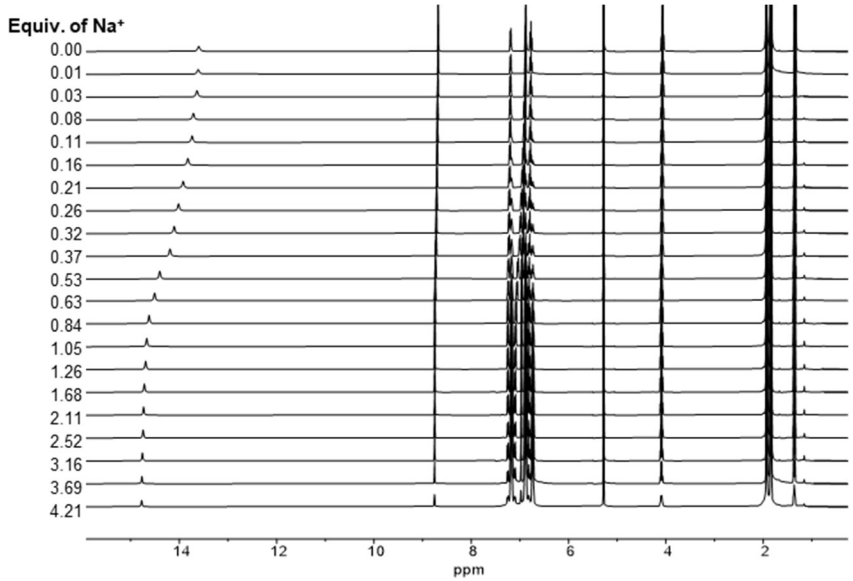

Fig. S49. Stacked ^{1}H NMR (400 MHz, DCM-d_2/MeCN-d_3, 25 ºC) spectra for the titration of **3b** with Na·BPh$_4$.

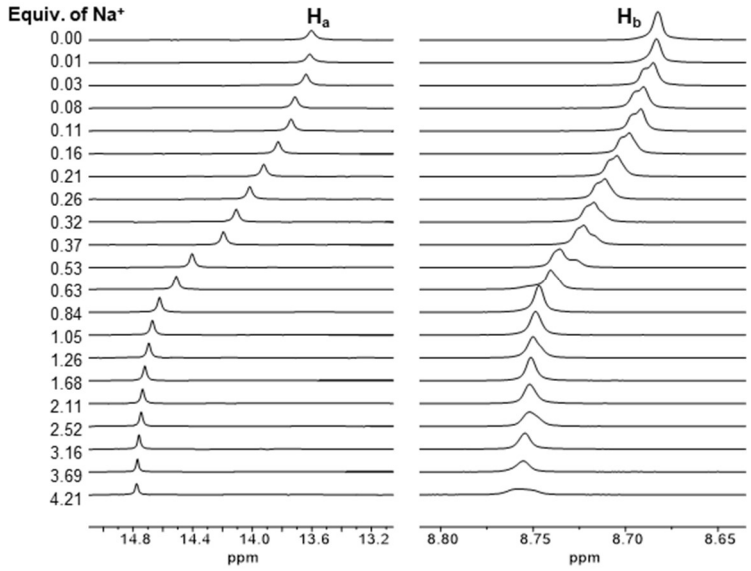

Fig. S50. Partial Stacked ^{1}H NMR (400 MHz, DCM-d_2/MeCN-d_3, 25 ºC) spectra for the titration of **3b** with Na·BPh$_4$. Specifically highlighting H_a and H_b.

At the early stages of the titration for **3b**+Na^+, two overlapping peaks appear for H_b. This is likely a result of 1:1 and 2:1 complexes being present.

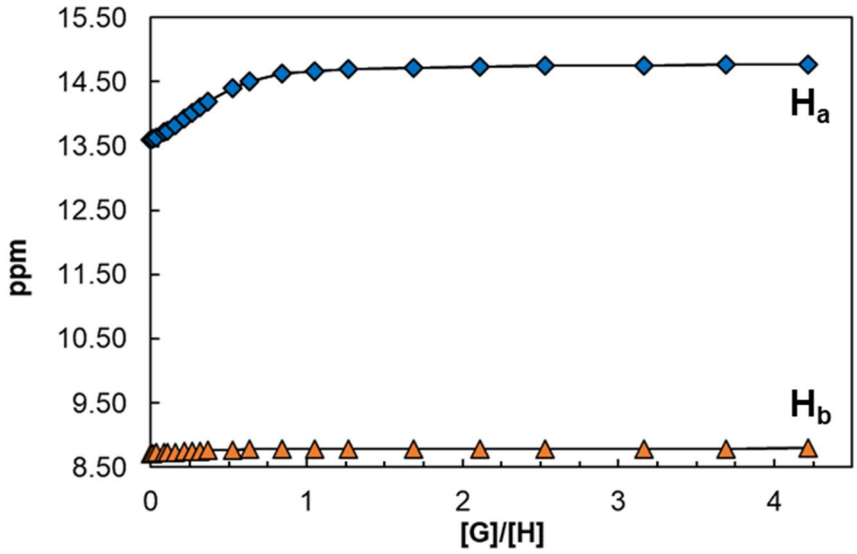

Fig. S51. ^{1}H NMR isotherms for resonances H_a and H_b obtained from the titration of **3b** with Na·BPh$_4$. Markers for experimental data, trend line for fit data.

NMR titration of 3b with K·BPh$_4$

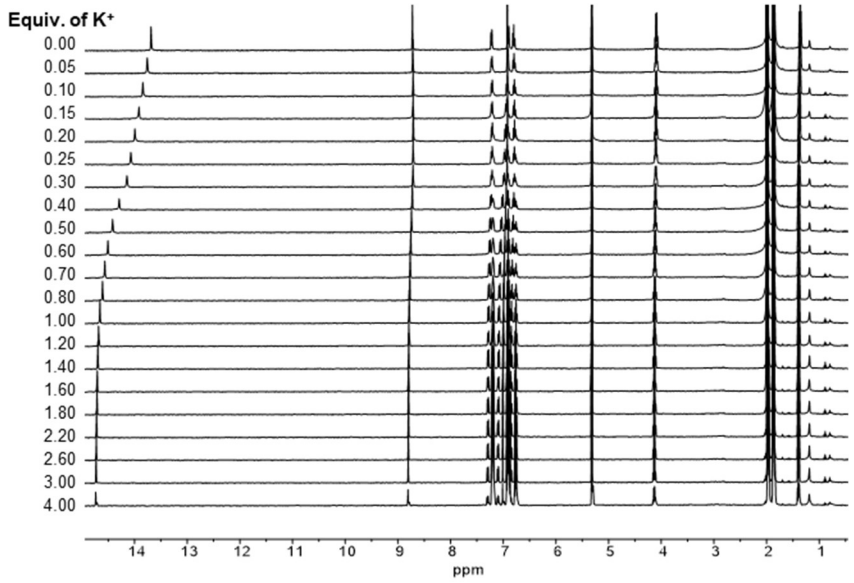

Fig. S52. Stacked ^{1}H NMR (400 MHz, DCM-d_2/MeCN-d_3, 25 ºC) spectra for the titration of **3b** with K·BPh$_4$.

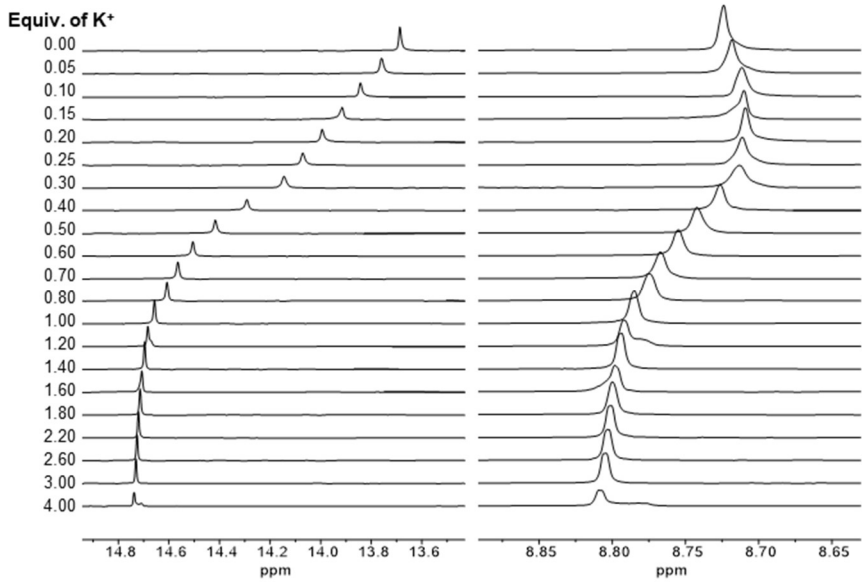

Fig. S53. Partial Stacked ^{1}H NMR (400 MHz, DCM-d_2/MeCN-d_3, 25 ºC) spectra for the titration of **3b** with K·BPh$_4$. Specifically highlighting H_a and H_b.

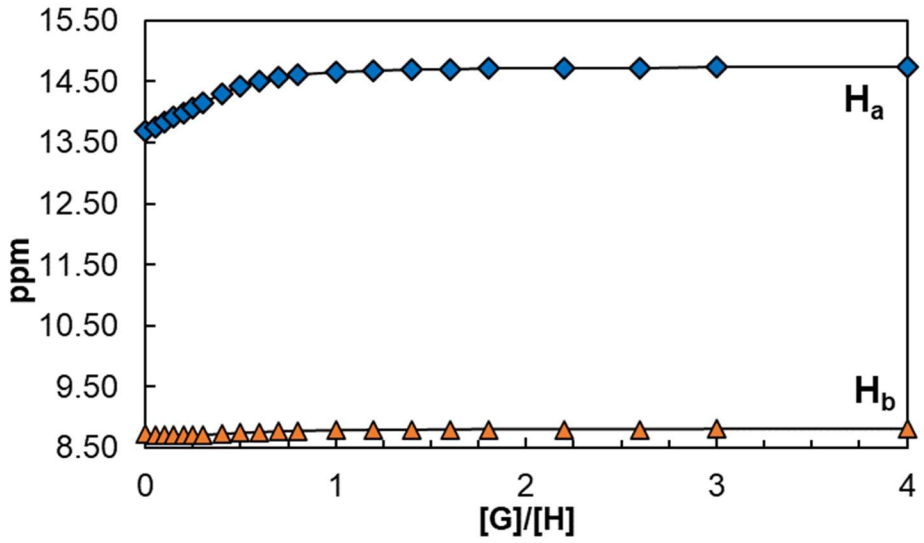

Fig. S54. ^{1}H NMR isotherms for resonances H_a and H_b obtained from the titration of **3b** with K·BPh_4. Markers for experimental data, trend line for fit data.

Titration and guest binding stoichiometry discussion

Although compound **3b** is quite simple in structure, the guest binding was not straight forward. For instance, we attempted to find a guest binding stoichiometry using the Job plot method (commonly used), however this did not work. This can be seen through ^{1}H Job plot analysis (Fig. S27). Theoretically, the maxima will occur at a mole fraction (χ) which corresponds to the host-guest stoichiometry. From these experiments it seems **3b+Na$^+$** and **3b+K$^+$** form 1:1 complexes, indicated by maxima occurring at $\chi_{guest}{}^+$ = 0.5. In contrast, the maxima for **3b+Rb$^+$** appears at $\chi_{Rb}{}^+$ = 0.33, which is consistent with a 2:1 host-guest complex. The Job plot obtained for **3b+Li$^+$** did not show a clear maximum ($\chi_{Li}{}^+$ = 0.33 & 0.50), which implies both 1:1 and 2:1 complexes are present. When the maxima are not sharp, the exact binding stoichiometry cannot be determined reliably. We also performed Job's method on **3b** and the guest cations using UV-vis spectroscopy (Fig. S28). The results of these measurements showed only 1:1 complexes for all host-guest systems, which contradicts the ^{1}H NMR spectroscopy experiments. Limits of Job plot analysis have been recently discussed in the literature,[9,10] where researchers overly rely on the method solely for host-guest stoichiometry detection. Thordarson,[9] and Jurczak,[10] both mentions that unreliable results can be obtained by having dilute samples.

There are other methods that can be used to determine host-guest stoichiometry, for instance A) comparison of K_a values at different concentrations,[11] B) determination of K_a through different methods (*e.g.* NMR, UV-vis, *ect.*), C) residual mapping, [12,13] D) the slope ratio method,[14] and E) the mole ratio method. We chose to use of combination of K_a determination through different methods and residual mapping.[12]

Rationally by examining the size of host **3b** the formation of 1:2, 1:3, or higher order complexes are not possible. The 18-crown-6-like cavity of **3b** can only interact with one guest at a time. However, 2:1 or 3:1 complexes are also possible, through sandwich like binding. This type of binding becomes more likely, as we increase the ionic radii of the guest.

As an example we modelled the binding of **3b+Li$^+$** to the 1:1, and 1:2 (none, additive, noncooperative, and statistical) binding models using BindFit,[15] which we highlight in the following section.

Modelling of 3b+Li$^+$ to several binding stoichiometries.

Note although we collected data to [Guest]/[Host] of 50 equiv., we completed the analysis from 0 to 10 equiv., because these later points diluted the sample too much leading to concentration effects and non-linear behaviour. This large change in host-guest complex concentration made it difficult to measure one discrete complex.

Below we have modelled the binding isotherms for 1:1, 1:2, and 2:1 host-guest complexes for **3b+Li$^+$**. In the 1:2 and 2:1 complex cases, the first binding event (denoted by K_{11}) can have an additive, noncooperative, statistical, or no (full) effect on the second binding (K_{12} or K_{21}). These definitions were from earlier publications,[9,12,16] and are based on the relationship between successive association constants (K_{11} and K_{21}) and absorptivity ($\varepsilon_{\Delta HG}$ vs $\varepsilon\Delta_{H2G}$) of the resulting complexes. For more information see those aforementioned publications.[9,12,16] We performed each titration twice, to confirm that no large discrepancies between the data sets were seen. The UV-vis titration isotherms using absorbances at 500, 360, and 320 nm, fit to a 1:1 (Fig. S59), 1:2 (Fig. S60), and 2:1(Fig. S61) model are shown below.

When **3b+Li$^+$** was fit to a 1:1 model, we found that modelling 500, 360, and 320 nm resulted in no solution being found. Thus, we had to reattempt the fitting using only the absorbance data at 500 nm. Although the model seems to have a low error (*ca.* 5.5 %) (Fig. S59A), having two absorption bands that could not be used in calculations makes this binding stoichiometry unlikely. Also, the residuals that result from fitting titration data to a model should in theory be random in nature, as these deviations result from non-systematic errors. However, the residual plot in Fig. S59B seems to have a sinusoidal shape, which results when the fitting does not take into account some of the titration data.[10,17]

Next, we examined the possibility of a 1:2 complex (one host and two guests) for **3b+Li$^+$**. The full (Fig. S60A) and additive (Fig. S60E) models, are both clearly not the correct fitting. Both fittings result in sinusoidal shaped residuals (Fig. S60D&F) and large errors. Also, the calculated association constant for the second binding event (K_{12}) using the full model is negative (K_{12} = -58.6 M^{-1}), which is impossible. The 1:2 noncooperative model (Fig. S60B) seems to be the most likely, because moderately sized K_{11} (9550 M^{-1}), and very small error (*ca.* 2.1 %). Also, upon examinations of the residual plot (Fig. S60E), the intensities are extremely low and appear random.

We chose to model 2:1 (two hosts one guest) complex binding isotherms (Fig. S61A,C,E,&G) and residuals (Fig. S61B,D,&H) for **3b-Li$^+$** as well. The 2:1 additive and full models, just like the aforementioned 1:2 cases, had large, ordered residual plots, implying improper fitting of data. Unsurprisingly, the fitting 2:1 using the noncooperative model is very similar

to the 1:2 (noncooperative) data set. This can be seen when comparing the residual plots Fig. S60H and Fig. S61H, where the residuals seem to match. However, the 2:1 noncooperative complex is much more likely, owing to the small size of host **3b** and the 18-crown-6 like cavity.

UV-vis titration spectra

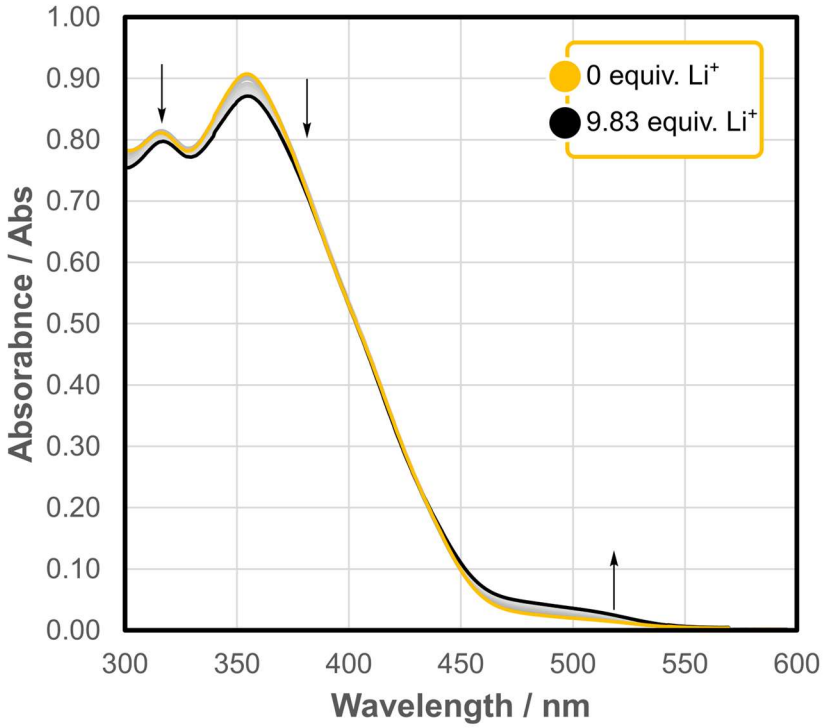

Fig. S55. Titration of **3b** with Li·BPh_4(1,2-DME)$_3$ in DCM/MeCN. Colour code: orange (0 equiv. Li^+) and black (9.83 equiv. Li^+).

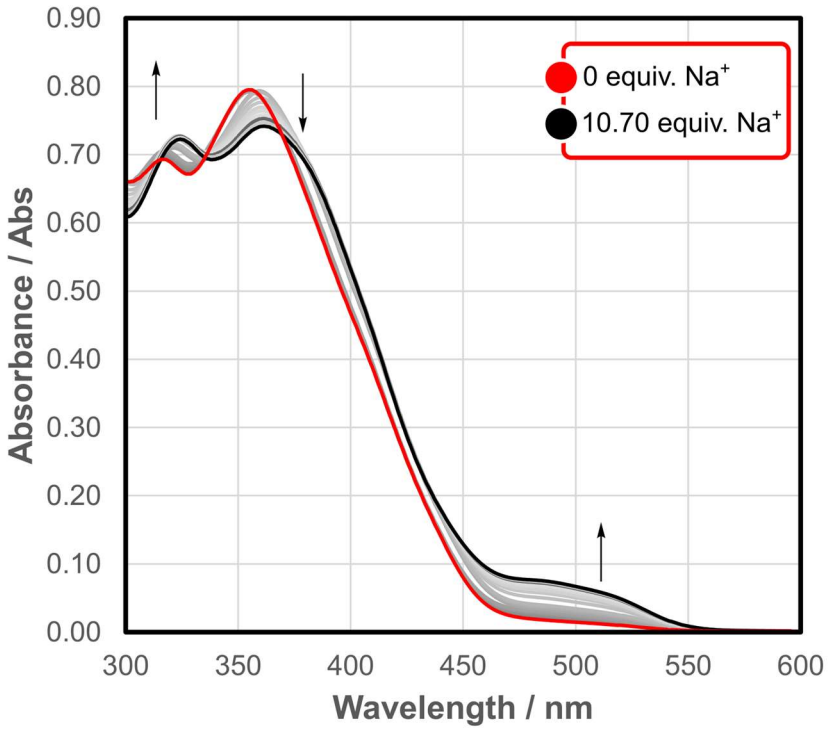

Fig. S56. Titration of **3b** with Na·BPh_4 in DCM/MeCN. Colour code: red (0 equiv. Na^+) and black (10.70 equiv. Na^+).

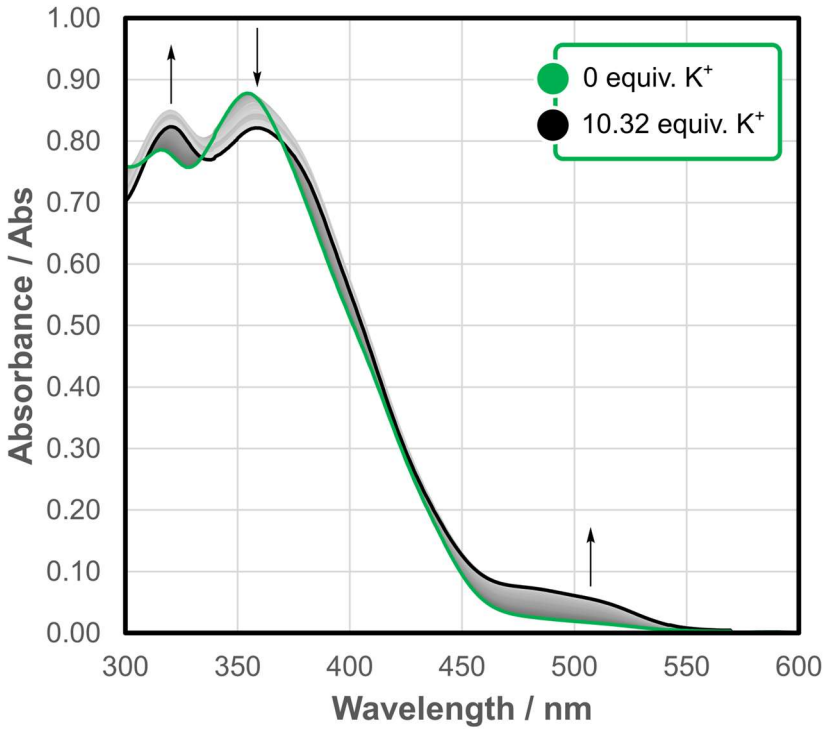

Fig. S57. Titration of **3b** with K·BPh_4 in DCM/MeCN. Colour code: green (0 equiv. K^+) and black (10.32 equiv. K^+).

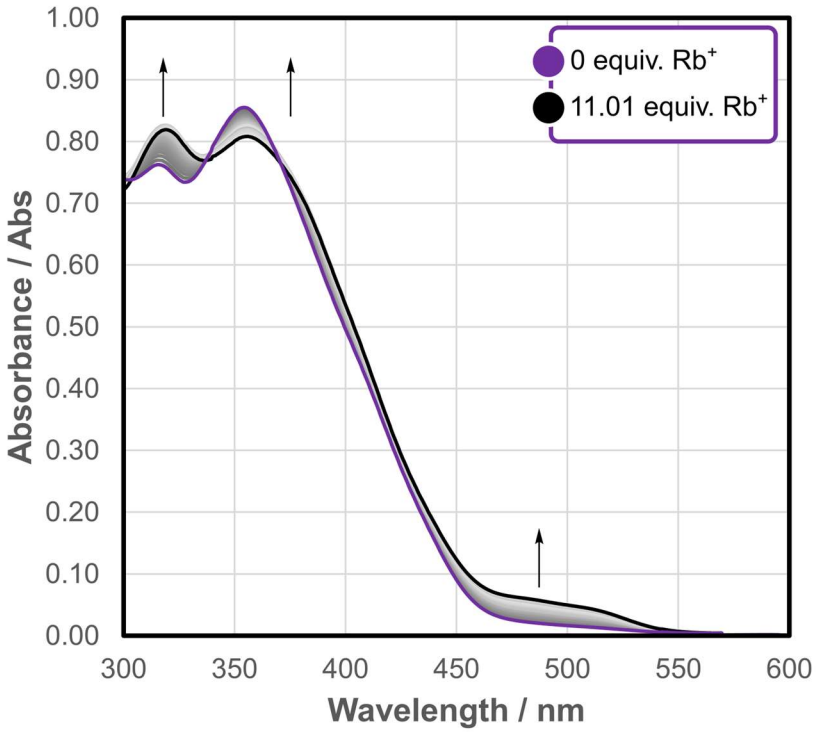

Fig. S58. Titration of **3b** with $Rb{\cdot}BPh_4$ in MeCN. Colour code: purple (0 equiv. Rb^+) and black (11.01 equiv. Rb^+).

Titration isotherms

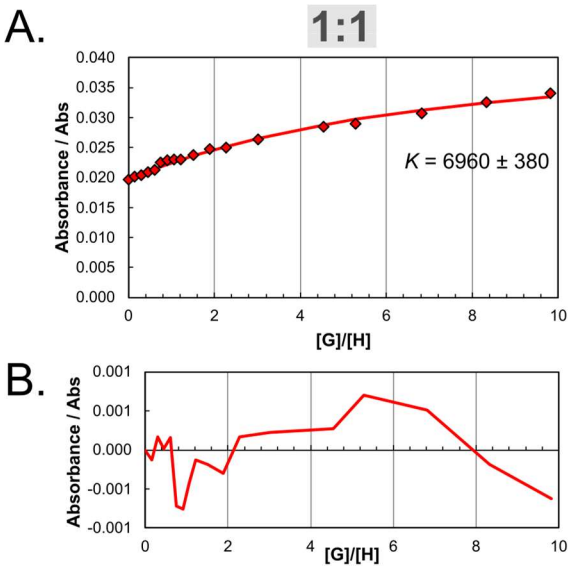

Fig. S59. A) UV-vis binding isotherm, and B) residual plot for **3b+Li$^+$** fit to a 1:1 complex. Colour code (red = 500 nm).

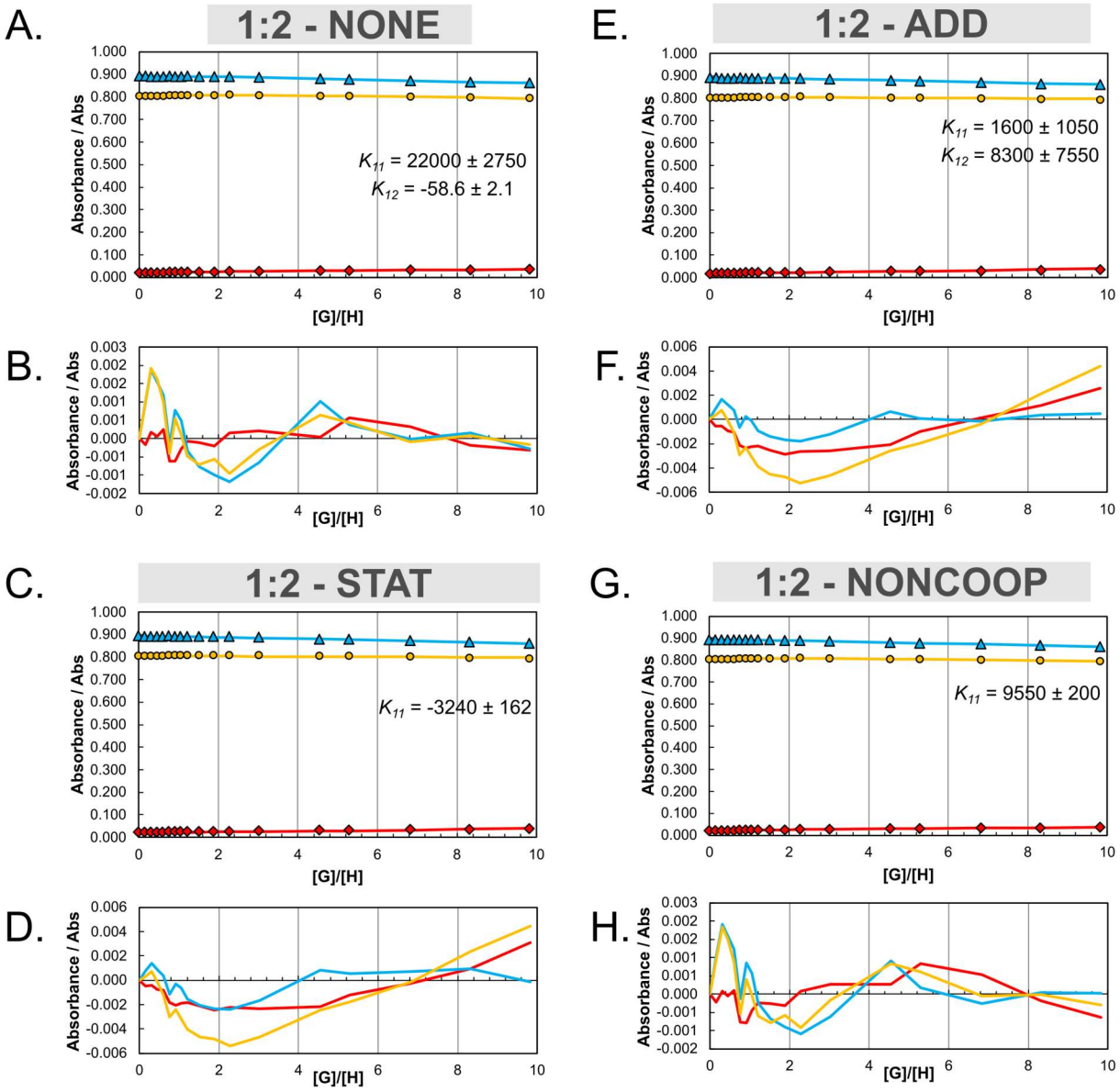

Fig. S60. UV-vis binding isotherms for **3b+Li⁺** fit to a 1:2 binding model. A) None (full) binding isotherm, B) None (full) binding residuals, C) statistical binding isotherm, D) statistical binding residuals, E) additive binding isotherm, F) additive cooperativity binding residuals, G) noncooperative binding isotherm, and H) noncooperative binding residuals. Colour code (red = 500 nm, blue = 360 nm, orange 320 nm).

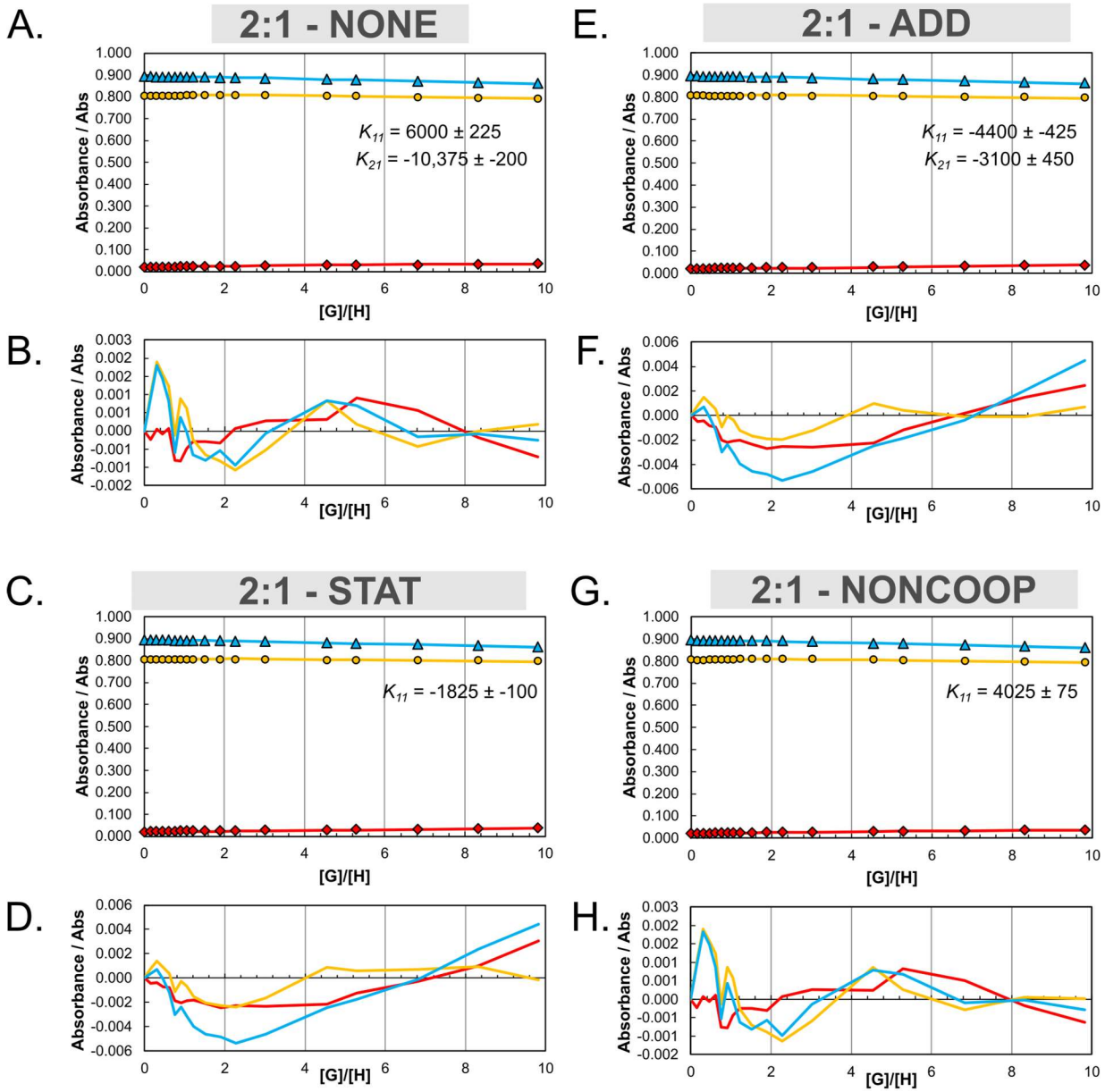

Fig. S61. UV-vis binding isotherms for **3b+Li⁺** fit to a 2:1 binding model. A) None (full) binding isotherm, B) None (full) binding residuals, C) statistical binding isotherm, D) statistical binding residuals, E) additive binding isotherm, F) additive cooperativity binding residuals, G) noncooperative binding isotherm, and H) noncooperative binding residuals. Colour code (red = 500 nm, blue = 360 nm, orange 320 nm).

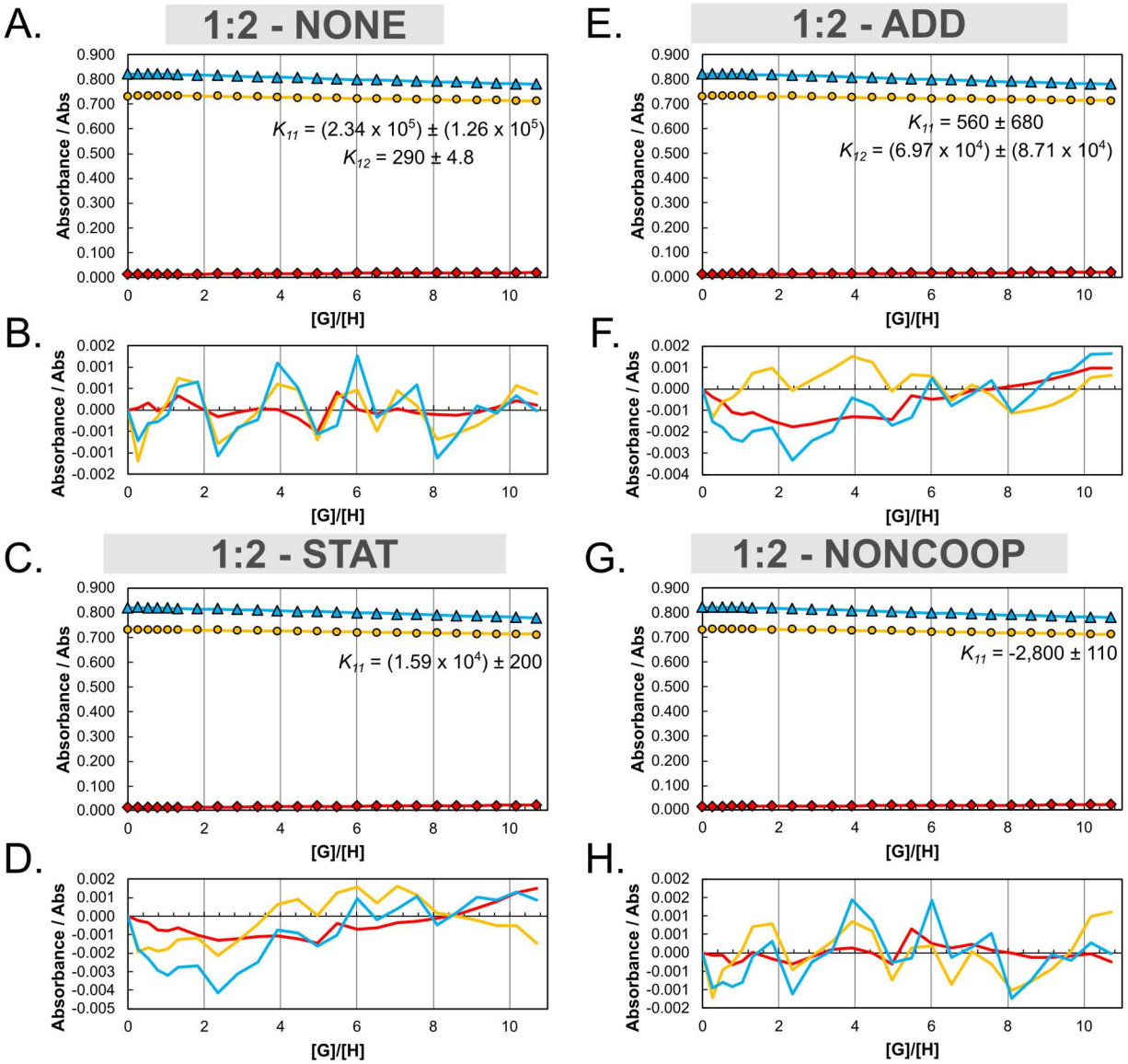

Fig. S62. UV-vis binding isotherms for **3b+Na⁺** fit to a 1:2 binding model. A) None (full) binding isotherm, B) None (full) binding residuals, C) statistical binding isotherm, D) statistical binding residuals, E) additive binding isotherm, F) additive cooperativity binding residuals, G) noncooperative binding isotherm, and H) noncooperative binding residuals. Colour code (red = 500 nm, blue = 360 nm, orange 320 nm).

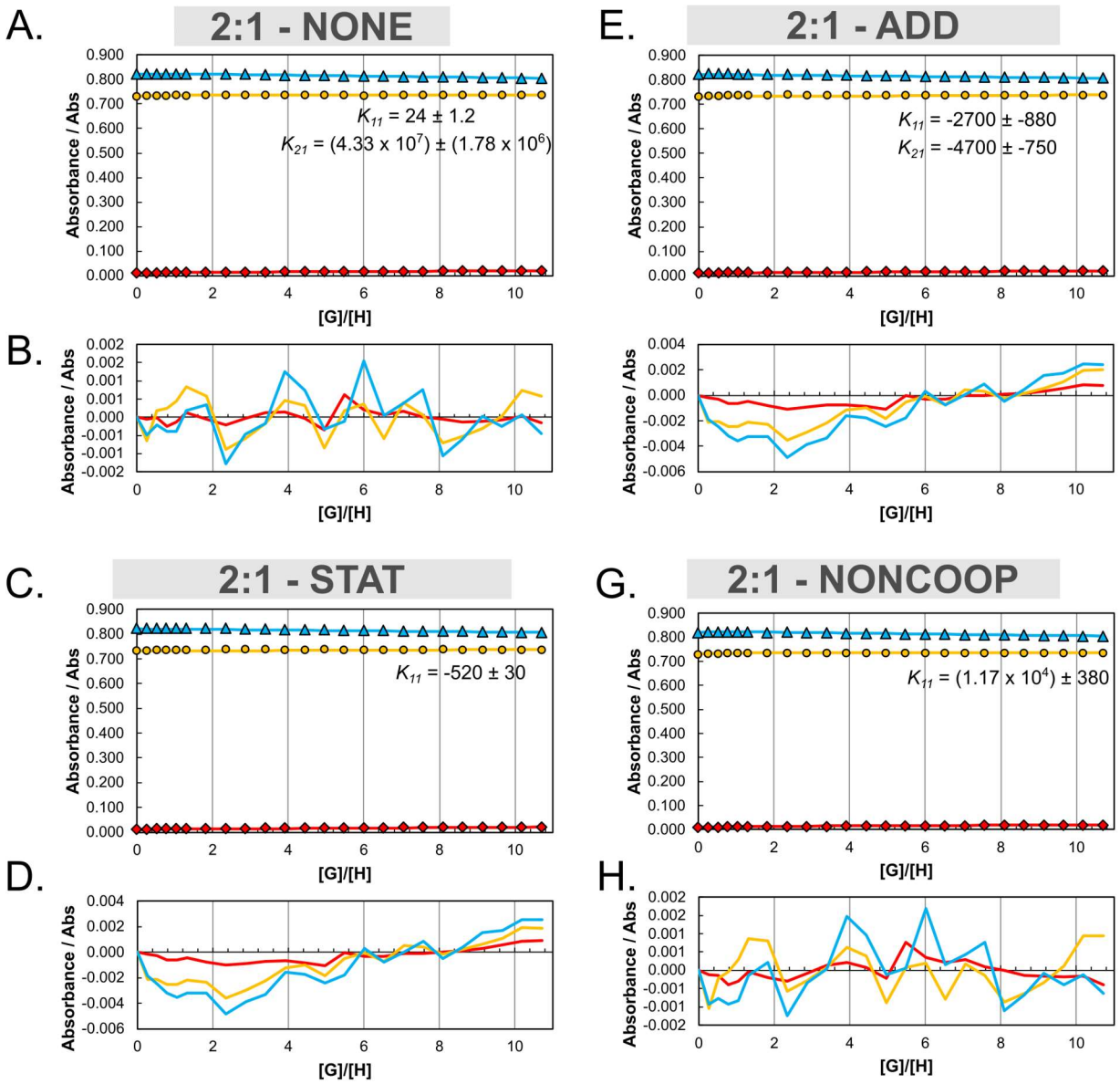

Fig. S63. UV-vis binding isotherms for **3b+Na⁺** fit to a 2:1 binding model. A) None (full) binding isotherm, B) None (full) binding residuals, C) statistical binding isotherm, D) statistical binding residuals, E) additive binding isotherm, F) additive cooperativity binding residuals, G) noncooperative binding isotherm, and H) noncooperative binding residuals. Colour code (red = 500 nm, blue = 360 nm, orange 320 nm).

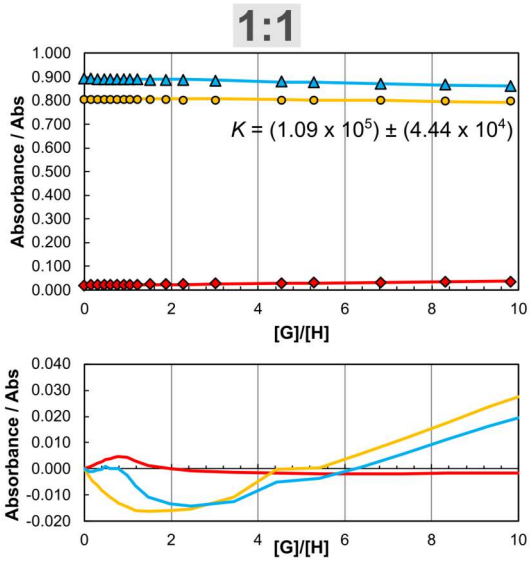

Fig. S64. UV-vis binding isotherms and residual plot for **3b+K⁺** fit to a 1:1 binding model. Colour code (red = 500 nm, blue = 360 nm, orange 320 nm).

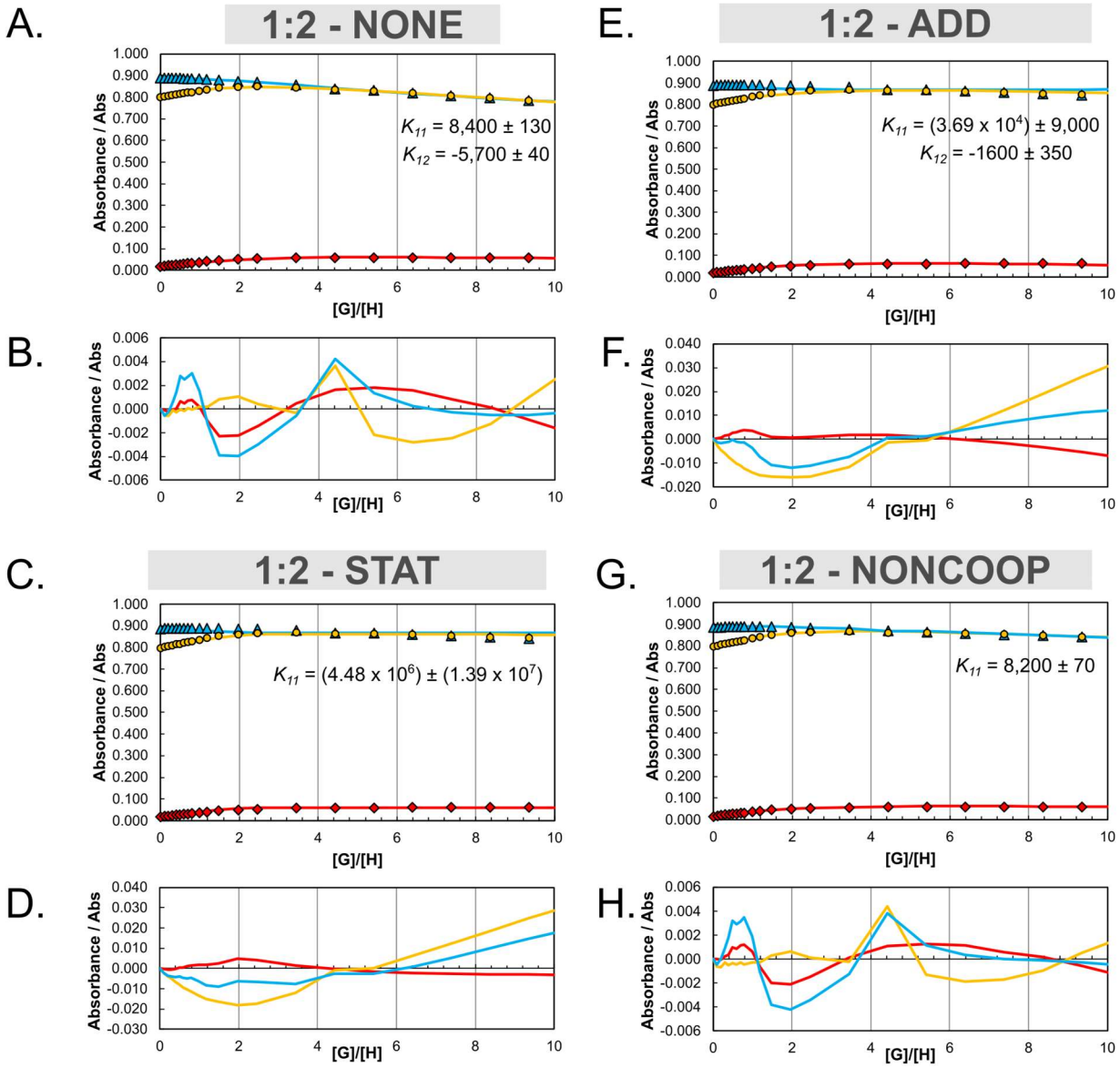

Fig. S65. UV-vis binding isotherms for **3b+K⁺** fit to a 1:2 binding model. A) None (full) binding isotherm, B) None (full) binding residuals, C) statistical binding isotherm, D) statistical binding residuals, E) additive binding isotherm, F) additive cooperativity binding residuals, G) noncooperative binding isotherm, and H) noncooperative binding residuals. Colour code (red = 500 nm, blue = 360 nm, orange 320 nm).

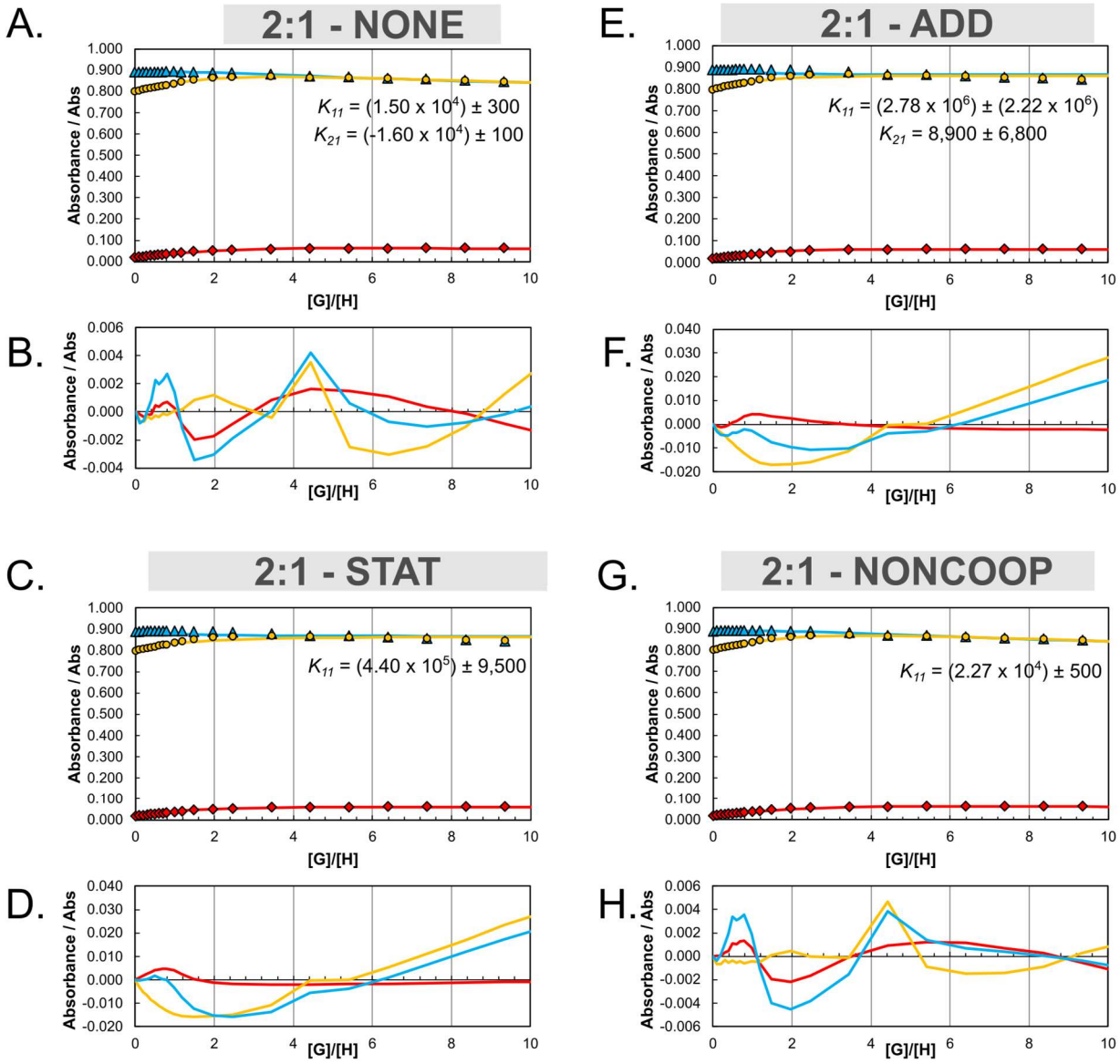

Fig. S66. UV-vis binding isotherms for **3b+K⁺** fit to a 2:1 binding model A) None (full) binding isotherm, B) None (full) binding residuals, C) statistical binding isotherm, D) statistical binding residuals, E) additive binding isotherm, F) additive cooperativity binding residuals, G) noncooperative binding isotherm, and H) noncooperative binding residuals. Colour code (red = 500 nm, blue = 360 nm, orange 320 nm).

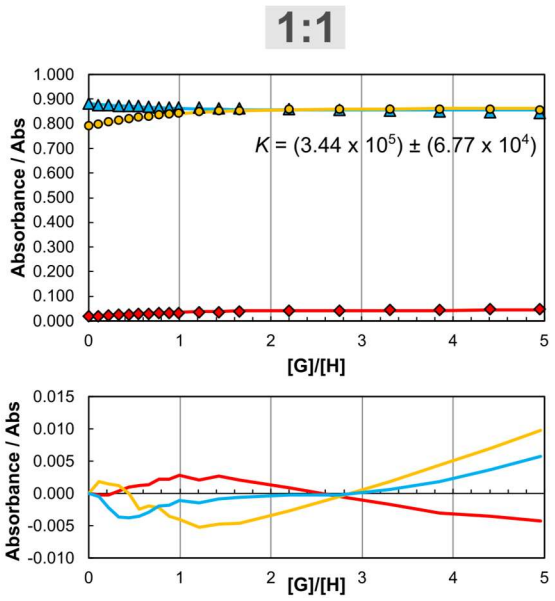

Fig. S67. UV-vis binding isotherms and residual plot for **3b+Rb$^+$** fit to a 1:1 binding model. Colour code (red = 500 nm, blue = 360 nm, orange 320 nm).

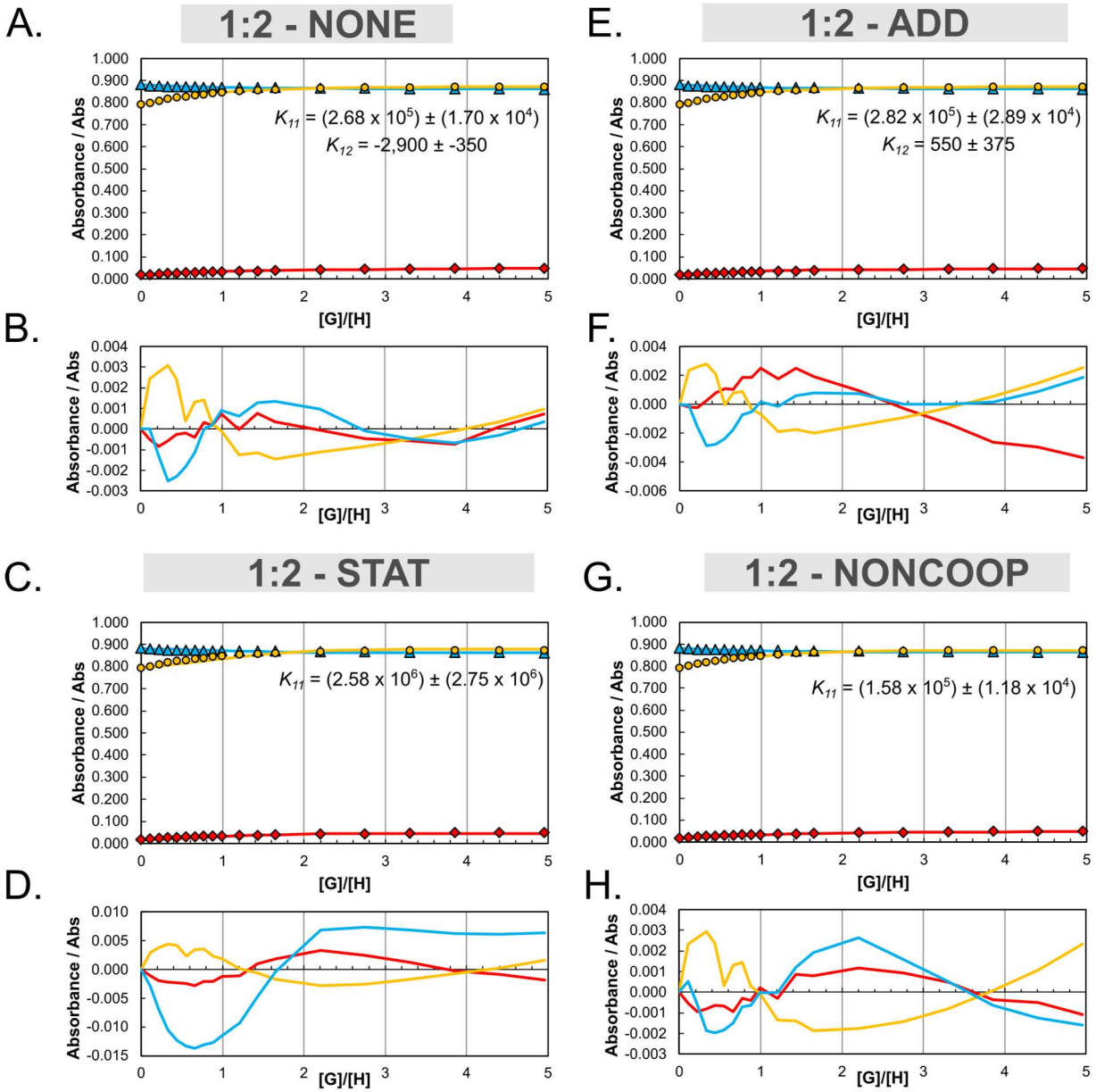

Fig. S68. UV-vis binding isotherms for **3b+Rb$^+$** fit to a 1:2 binding model. A) None (full) binding isotherm, B) None (full) binding residuals, C) statistical binding isotherm, D) statistical binding residuals, E) additive binding isotherm, F) additive cooperativity binding residuals, G) noncooperative binding isotherm, and H) noncooperative binding residuals. Colour code (red = 500 nm, blue = 360 nm, orange 320 nm).

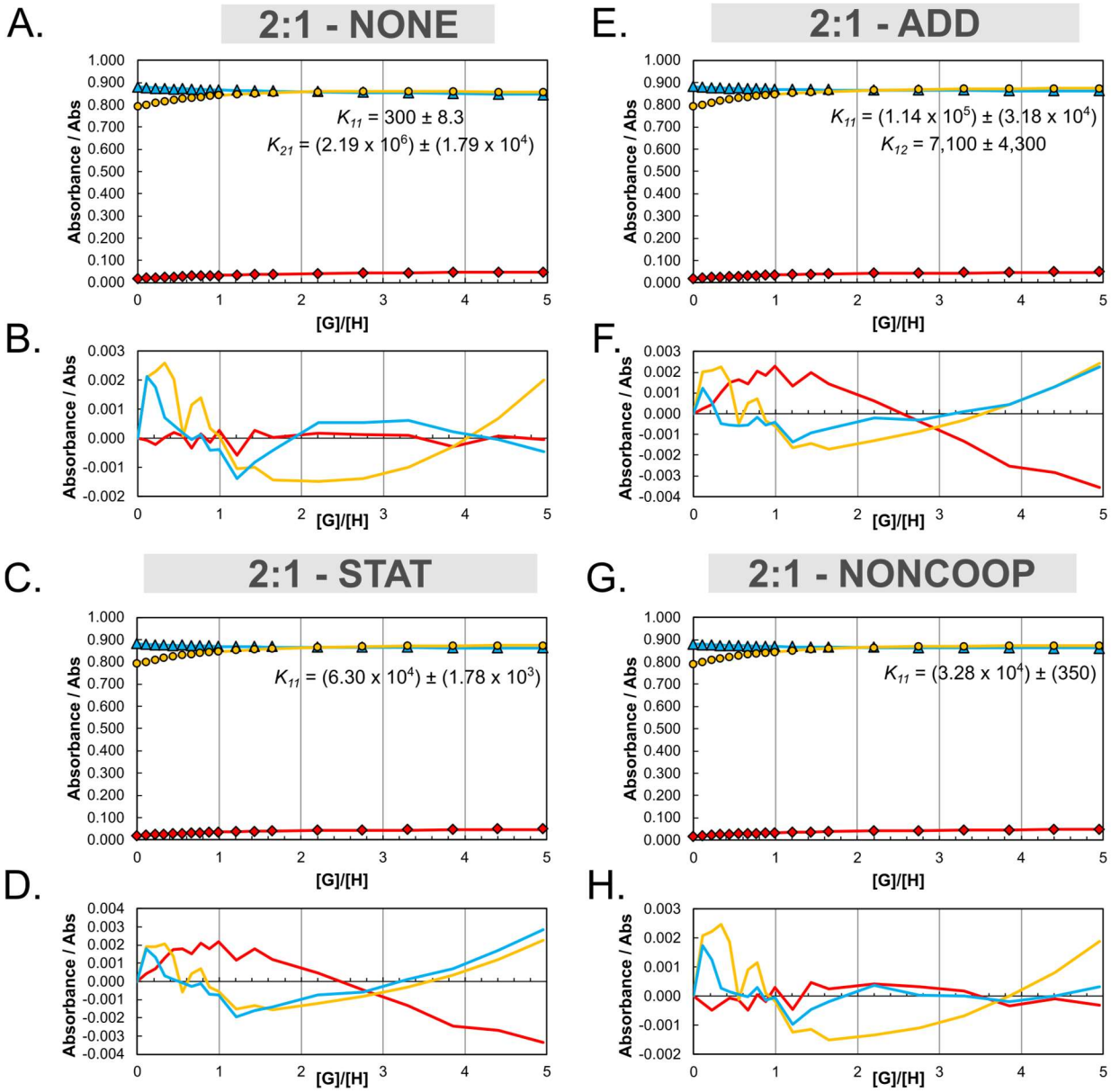

Fig. S69. UV-vis binding isotherms for **3b+Rb$^+$** fit to a 2:1 binding model. A) None (full) binding isotherm, B) None (full) binding residuals, C) statistical binding isotherm, D) statistical binding residuals, E) additive binding isotherm, F) additive cooperativity binding residuals, G) noncooperative binding isotherm, and H) noncooperative binding residuals. Colour code (red = 500 nm, blue = 360 nm, orange 320 nm).

Table S1. Association constants for **3b+Li**$^+$ calculated using various models.

Binding model	First association constant (M^{-1})	Second association constant (M^{-1})	Error (%)
1 to 1	6960 ± 380	n.a	5.5
1 to 2 – *None (full)*	22000 ± 2750	-58.6 ± 2.1	12.5, 3.6
1 to 2 – *Additive*	1600 ± 1050	8300 ± 7550	65.6, 90.1
1 to 2 – *Noncooperative*	9550 ± 200	a	2.1
1 to 2 – *Statistical*	-3240 ± 162	a	5.0
2 to 1 - *None (full)*	-6000 ± 225	-10,375 ± - 200	3.8
2 to 1 – *Additive*	-4400 ± -425	-3100 ± 450	9.7, 14.5
2 to 1 – *Noncooperative*	4025 ± 75	b	1.9
2 to 1 – *Statistical*	-1825 ± -100	b	-5.5

[a] $K_{11} = K_{12}$. [b] $K_{11} = K_{21}$. [c] Most likely complex (lowest error, no order in the residuals, association constants which are possible given the binding mode).

Table S2. Association constants for **3b+Na**$^+$ calculated using various models.

Binding model	First association constant (M^{-1})	Second association constant (M^{-1})	Error (%)
1 to 1	Failed	n.a	
1 to 2 – *None (full)*	2.34×10^5	290	53.7, 1.7
1 to 2 – *Additive*	560	6.97×10^4	121.7, 125.0
1 to 2 – *Noncooperative*	-2800	a	-1.7,
1 to 2 – *Statistical*	1.59×10^4	a	1.0
		a	
2 to 1 - *None (full)*	24 ± 1.2	4.33×10^7, 1.78×10^6	5, 4.1
2 to 1 – *Additive*	-2700 ± -880	-4700 ± -750	32.6, 16.0
2 to 1 – *Noncooperative*	1.17×10^4 ± 380	b	3.2
2 to 1 – *Statistical*	-520 ± 30	b	5.7

[a] $K_{11} = K_{12}$. [b] $K_{11} = K_{21}$. [c] Most likely complex (lowest error, no order in the residuals, association constants which are possible given the binding mode).

Table S3. Association constants for **3b+K**$^{+}$ calculated using various models.

Binding model	First association constant (M^{-1})	Second association constant (M^{-1})	Error (%)
1 to 1	1.09 x 10^5 ± 4.44 x 10^4	n.a	40.7
1 to 2 – *None (full)*	8400 ± 130	-5700 ± 40	1.5, 0.7
1 to 2 – *Additive*	3.69 x 10^4, ± 9000	-1600 ± 350	24.3, -21.9
1 to 2 – *Noncooperative*	8200 ± 70	a	0.85
1 to 2 – *Statistical*	4.48 x 10^6 ± 1.39 x 10^7	a	310
2 to 1 - *None (full)*	1.50 x 10^4 ± 300	-1.60 x 10^4 ± 100	2.0, -0.63
2 to 1 – *Additive*	2.78 x 10^6 ± 2.22 x 10^6	8900 ± 6800	79.8, 76.4
2 to 1 – *Noncooperative*	2.27 x 10^4 ± 500	b	2.2
2 to 1 – *Statistical*	4.40 x 10^5 ± 9500	b	2.16

[a] $K_{11} = K_{12}$. [b] $K_{11} = K_{21}$. [c] Most likely complex (lowest error, no order in the residuals, association constants which are possible given the binding mode).

Table S4. Association constants for **3b+Rb**$^{+}$ calculated using various models.

Binding model	First association constant (M^{-1})	Second association constant (M^{-1})	Error (%)
1 to 1	3.44 x 10^5	n.a	19.7
1 to 2 – *None (full)*	2.68 x 10^5	-2900	6.3, -12.8
1 to 2 – *Additive*	2.82 x 10^5	550	10.3, 68.3
1 to 2 – *Noncooperative*	2.58 x 10^6	a	107.5
1 to 2 – *Statistical*	1.58 x 10^5	a	7.46
2 to 1 - *None (full)*	300	2.19 x 10^6	2.6, 0.8
2 to 1 – *Additive*	1.14 x 10^5	7100	28.9, 60.6
2 to 1 – *Noncooperative*	3.28 x 10^4	b	1.01
2 to 1 – *Statistical*	6.30 x 10^4	b	2.8

[a] $K_{11} = K_{12}$. [b] $K_{11} = K_{21}$. [c] Most likely complex (lowest error, no order in the residuals, association constants which are possible given the binding mode).

References

1 S. Akine, F. Utsuno and T. Nabeshima, Highly efficient regulation of cation recognition and promotion of self-assembly by metalation of a macrocyclic bis(N_2O_2) ligand with nickel(II), *Chem. Commun.*, 2010, **46**, 1029–1031.

2 Bruker. APEX3. Bruker AXS Inc.: Madison, Wisconsin, USA. 2012.

3 Bruker. SAINT. Bruker AXS Inc.: Madison, Wisconsin, USA. 2012.

4 G. M. Sheldrick, SHELXT - Integrated space-group and crystal-structure determination, *Acta Crystallogr., Sect. A: Found. Crystallogr.*, 2015, **71**, 3–8.

5 G. M. Sheldrick, Crystal structure refinement with SHELXL, *Acta Crystallogr., Sect. C: Cryst. Struct. Commun.*, 2015, **71**, 3–8.

6 H. Puschmann, OLEX2: a complete structure solution, refinement and analysis program, *J. Appl. Crystallogr.*, 2009, **42**, 330–341.

7 D. C. Palmer, CrystalMaker. CrystalMaker Software Ltd: Begbroke, Oxfordshire, England 2014.

8 V. Petříček, M. Dušek and J. Plášil, Crystallographic computing system Jana2006: solution and refinement of twinned structures, *Zeitschrift für Krist. - Cryst. Mater.*, 2016, **231**, 583–599.

9 D. B. Hibbert and P. Thordarson, The death of the Job plot, transparency, open science and online tools, uncertainty estimation methods and other developments in supramolecular chemistry data analysis, *Chem. Commun.*, 2016, **52**, 12792–12805.

10 F. Ulatowski, K. Dąbrowa, T. Bałakier and J. Jurczak, Recognizing the Limited Applicability of Job Plots in Studying Host–Guest Interactions in Supramolecular Chemistry, *J. Org. Chem.*, 2016, **81**, 1746–1756.

11 B. Perlmutter-Hayman, Cooperative binding to macromolecules. A formal approach, *Acc. Chem. Res.*, 1986, **19**, 90–96.

12 P. Thordarson, Determining association constants from titration experiments in supramolecular chemistry, *Chem. Soc. Rev.*, 2011, **40**, 1205–1323.

13 D. B. Hibbert and P. Thordarson, The death of the Job plot, transparency, open science and online tools, uncertainty estimation methods and other developments in supramolecular chemistry data analysis, *Chem. Commun.*, 2016, **52**, 12792–12805.

14 K. A. Connors and J. A. Mollica JR., Theoretical analysis of comparative studies of complex formation: Solubility, spectral, and kinetic techniques, *J. Pharm. Sci.*, 1966, **55**, 772–780.

15 P. Thordarson, supramolecular.org. Accessed April 24, 2022.

16 E. N. W. Howe, M. Bhadbhade and P. Thordarson, Cooperativity and Complexity in the Binding of Anions and Cations to a Tetratopic Ion-Pair Host, *J. Am. Chem. Soc.*, 2014, **136**, 7505–7516.

17 C. A. Schalley, *Analytical Methods in Supramolecular Chemistry*, John Wiley & Sons, Weinheim, 2nd edn., 2012.